Mapping membrane receptor distribution on resting platelets combining Expansion Microscopy and fluorescence confocal microscopy

***

Kartierung der Membranrezeptorverteilung auf nicht-aktivierten Blutplättchen mithilfe der Kombination aus Expansionsmikroskopie und konfokaler Fluoreszenzmikroskopie

Doctoral thesis for a doctoral degree

at the Graduate School of Life Sciences,

Julius-Maximilian-Universität Würzburg,

Section Biomedicine

Submitted by

Sophia Edith Maier

from Traunstein, Germany

München 2022

” I am enough of the artist to draw freely upon my imagination.
Imagination is more important than knowledge.
Knowledge is limited. Imagination encircles the world. “
Albert Einstein

submitted on:

……

Members of the Thesis Committee

Chairperson:	Prof. Dr. Philip Tovote
Primary supervisor:	Prof. Dr. Katrin Heinze
Supervisor (second):	Prof. Dr. Harald Schulze
Supervisor (third):	Prof. Dr. Markus Sauer

Date of Public Defense: ……

Date of Receipt of Certificates: ……

Abstract

Stroke and myocardial infarction are the most prominent and severe consequences of pathological thrombus formation. For prevention and/or treatment of thrombotic events there is a variety of anti-coagulation and antiplatelet medication that all have one side effect in common: the increased risk of bleeding. To design drugs that only intervene in the unwanted aggregation process but do not disturb general hemostasis, it is crucial to decipher the exact clotting pathway which has not been fully understood yet. Platelet membrane receptors play a vital role in the clotting pathway and, thus, the aim of this work is to establish a method to elucidate the interactions, clustering, and reorganization of involved membrane receptors such as GPIIb/IIIa and GPIX as part of the GPIb-IX-V complex. The special challenges regarding visualizing membrane receptor interactions on blood platelets are the high abundancy of the first and the small size of the latter (1—3µm of diameter). The resolution limit of conventional fluorescence microscopy and even super-resolution approaches prevents the successful differentiation of densely packed receptors from one another. Here, this issue is approached with the combination of a recently developed technique called Expansion Microscopy (ExM). The image resolution of a conventional fluorescence microscope is enhanced by simply enlarging the sample physically and thus pulling the receptors apart from each other. This method requires a complex sample preparation and holds lots of obstacles such as variable or anisotropic expansion and low images contrast. To increase ExM accuracy and sensitivity for interrogating blood platelets, it needs optimized sample preparation as well as image analysis pipelines which are the main part of this thesis. The colocalization results show that either fourfold or tenfold expanded, resting platelets allow a clear distinction between dependent, clustered, and independent receptor organizations compared to unexpanded platelets. Combining dual-color Expansion and confocal fluorescence microscopy enables to image in the nanometer range identifying GPIIb/IIIa clustering in resting platelets – a pattern that may play a key role in the clotting pathway.

Zusammenfassung

Schlaganfall und Myokardinfarkt sind die wohl bekanntesten und schwerwiegendsten Folgen von pathologischer Thrombenbildung. Zur Vorbeugung und/oder ehandlung thrombotischer Ereignisse gibt es eine Vielzahl von Antiplättchen-Medikamenten wie Aspirin® oder Plavix®, denen allerdings eine Nebenwirkung gemein ist: das unerwünschte, erhöhte Blutungsrisiko. Um Medikamente zu entwickeln, die tatsächlich nur den Aggregationsprozess unterbinden, die generelle Blutstillung jedoch nicht unterbinden, ist es entscheidend, eine detaillierte Vorstellung der Signalkaskade der Plättchenadhesion und -aktivierung zu bekommen. Da diese bisher noch nicht vollständig verstanden wurde, soll eine Methode zur Aufklärung schneller Wechselwirkungen, Clusterbildung und Reorganisation von Plättchenrezeptoren wie GPIIb/IIIa und GPIX, als Teil des Rezeptorkomplex GPIb-IX-V, etabliert werden. Die besonderen Herausforderungen bei der Visualisierung von Wechselwirkungen von Membranrezeptoren auf Blutplättchen sind sowohl ihre hohe Dichte als auch die geringe Größe der Blutplättchen (1–3µm Durchmesser). Die Auflösungsgrenze der konventionellen Fluoreszenzmikroskopie sowie der superhochauflösenden-Mikroskopie ist nicht in der Lage dicht gepackte Rezeptoren voneinander zu unterscheiden. Eine kürzlich entwickelte Technik namens Expansionsmikroskopie (ExM) bietet hierfür einen Lösungsansatz: Die Bildauflösung von einem herkömmlichen Fluoreszenzmikroskop wird dadurch verbessert, dass Proben physikalisch vergrößert werden, sodass markierte Rezeptoren auseinanderdriften und besser voneinander unterschieden werden können. Dieses Verfahren erfordert eine komplexe Probenvorbereitung und birgt viele Unsicherheiten wie die Variabilität des Expansionsfaktors, die Isotropie des Expansionsprozesses sowie das niedrige Signal-Rausch-Verhältnis in den mikroskopischen Bildern. Um die Genauigkeit und Empfindlichkeit des Ansatzes auf seine Tauglichkeit zur Untersuchung nicht-aktivierter Blutplättchen zu überprüfen, wurde ein Arbeitsablauf für die optimale Probenvorbereitung entwickelt sowie auf wichtige Analysekriterien für die Kolokalisationsanalyse hingewiesen, welches den Hauptteil dieser Arbeit darstellt. Die Ergebnisse der Kolokalisationsanalyse zeigen, dass die vier– beziehungsweise zehnfache Expansion ruhender Blutplättchen eine eindeutige Unterscheidung zwischen abhängigen, geclusterten und unabhängigen Rezeptororganisationen im Vergleich zu nicht expandierten Blutplättchen erlaubt. Die Kombination aus ExM und konfokaler Fluoreszenzmikroskopie ermöglichte die Identifizierung von Clustern der GPIIb/IIIa-Rezeptoren in ruhenden Blutplättchen – ein Vorgang, der möglicherweise eine Schlüsselrolle in der Plättchenaggregation spielt.

Table of contents

Abbreviations **5**

List of Figures **6**

List of Tables **9**

1 Introduction **10**

1.1 Blood platelets in health and disease **10**

1.1.1 General role of blood platelets 10
1.1.2 Platelet adhesion and thrombus formation 11
1.1.3 Platelet receptors 14

1.2 Visualizing blood platelets down to the molecular level **15**

1.2.1 High resolution confocal fluorescence microscopy 15
1.2.2 Increasing the resolving power of the microscope: Super-resolution microscopy 20
1.2.3 Enhancing resolution by amplifying the sample: Expansion microscopy 22

1.3 Together or single: Colocalization as a key parameter to identify interaction zones in platelets **25**

1.3.1 Colocalization analysis as quantitative statistical measurement of the relationship between two molecules 25
1.3.2 Image acquisition and image pre-processing crucial for colocalization analysis 26
1.3.3 Quantifying colocalization based on pixel intensity: Pearson´s correlation coefficient (PCC) and Manders` overlap coefficient (MOC) 26

1.4 Aim of this study **29**

2 Materials and Methods **30**

2.1 Chemicals and materials **30**

2.1.1 Chemicals and reagents 30
2.1.2 Materials 31
2.1.3 Gel composition 4x and 10x Expansion 31
2.1.4 Buffers and stock solution 31
2.1.5 Antibodies 31

2.2 Methods **32**

2.2.1 Coverslip cleaning 32
2.2.2 Coverslip coating 32
2.2.3 Preparation of antibodies with trifunctional linkers and determination of Degree of Labeling (DOL) 32
2.2.4 Sample preparation 34
2.2.5 Preparation of expanded samples 35
2.2.6 Imaging unexpanded and expanded platelets 36
2.2.7 Microscope calibration 37
2.2.8 Guideline of sample preparation and colocalization analysis of resting, expanded platelets 41

3 Results 43

3.1 Optimized sample preparation 43

3.1.1 Experimental expansion factor and reproducibility 43
3.1.2 10x expansion: Optimized gel protocol 45
3.1.3 Comparison of the signal intensities in 4x and 10x expanded platelets 46
3.1.4 Maximizing signal retention by modified antibodies 47

3.2 Increase of colocalization analysis precision and comparison of colocalization test cases in unexpanded, 4x and 10x expanded resting platelets 48

3.2.1 Plotting the pixel signal intensities to look for linearity and determination of number of voxels (*N)* in platelets 48
3.2.2 Expanded platelets with small diameter and diagonal orientation distort colocalization results 49
3.2.3 Performance of high and weak colocalization test cases in unexpanded, 4x and 10x expanded resting platelets 50

4 Discussion 52

5 Future prospective 58

Appendix 59

A. Imaging settings 59
B. Macro file for applying distortion matrix 60
C. Statistics 60

Bibliography 61

Acknowledgement 67

Curriculum vitae 68

Affidavit 69

Eidesstattliche Erklärung 70

Abbreviations

AB	Antibody
A488	Alexa Fluor 488
A594	Alexa Fluor 594
Att488	Atto 488
APS	Ammonium persulfate
BSA	Bovine Serum Albumin
ddH_2O	Double-distilled water
(d)STORM	(direct) Stochastic Optical Reconstruction Microscopy
DMAA	N,N-dimethylacrylamide
DMSO	Dimethyl sulfoxide
DOL	Degree of labeling
EDTA	Ethylenediaminetetraacetic acid
ExM	Expansion Microscopy
GFP	Green Fluorescent Protein
GP	Glycoprotein
HEPES	4-(2-hydroxyethyl)-1- piperazineethanesulfonic acid
4HT	4-Hydroxy-TEMPO
KPS	Potassium persulfate
STORM	Stochastic Optical Reconstruction Microscopy
mAB	Monoclonal Antibody
MIT	Massachusetts Institute of Technology
MPV	Mean Platelet Volume
MOC	Manders´overlap coefficient
N_2	Nitrogen
NaCl	Sodium chloride
NA	Numerical Aperture
(f)PALM	(fluorescence) Photoactivation Localization Microscopy
PBS	Phosphate Buffered Saline
PCC	Pearson´s correlation coefficient
PGI_2	Prostacyclin
PRP	Platelet Rich Plasma
PSF	Point Spread Function
px	Pixel
rpm	Resolutions per minute
RT	Room Temperature
SIM	Structured Illumination Microscopy
SMLM	Single Molecule Localization Microscopy
SNR	Signal-to-Noise ratio
STED	Stimulated Emission Depletion
SRM	Super-resolution microscopy
TEMED	Tetramethylethylenediamin

List of Figures

Figure 1: Primary and secondary hemostasis. After sealing the vascular injury with a temporary platelet plug, the coagulation cascade provides a firm and stable thrombus to reconstruct the lesion. After tissue repair, the clot is broken down in a process called fibrinolysis. 11

Figure 2: Platelet adhesion (left) and activation (right). GPIb-IX-V first binds to the vWF, GPVI and GPIa/IIa are both binding to collagen. The adhesion of these receptors leads to the activation of platelets (marked by a star) and to a conformational change of GPIIb/IIIa. The secretion of fibrinogen, vWF, ADP and TXA_2 is a crucial part for further platelet activation and aggregation. **E** = Endothelial cell, **vWF** = von-Willebrand-Factor, **TF** = Tissue factor, **TXA_2** = Thrombaxene A_2............................... 12

Figure 3: Activated platelet aggregation leads to plug formation. The activation of GPIIb/IIIa enables the binding of vWF and Fibrinogen which function as bridges between activated platelets. The increasing aggregation promotes the formation of a platelet plug which prevents further bleeding. **E** = Endothelial cell, **vWF** = von-Willebrand-Factor, **TF** = Tissue factor, **TXA_2** = Thrombaxene A_2............ 13

Figure 4: Anti-GPIbα antibody (92H12) induces non-classical clotting. When adding the anti-GPIbα antibody *in vitro*, platelets aggregate (left panel) but do not get activated (right panel). This mechanism is called non-classical clotting. Images with courtesy of Bernhard Nieswandt. 14

Figure 5: Jablonski diagram shows principle of fluorescence. By excitation of the fluorophore to its excited electronic state S_1 and relaxation to the ground state S_0, fluorescence light will be emitted. The emitted light can then be captured with a sensor or a camera. 16

Figure 6: The Point-Spread Function (PSF) and lateral resolution limit of a light microscope. The blurry PSF of a point like emitter is ellipsoid shaped in the axial direction explaining the lower axial resolution (a). PSF widths larger apart from each other than the diffraction limit d_{lim} can be distinguished (b) while objects at a distance below the minimal distance d_{lim} cannot be resolved (c).. 17

Figure 7: Setup of a fluorescent confocal scanning microscope. a) The excitation lasers (blue and yellow) are directed via a dichroic mirror (DM) towards the scanning unit. The scanning unit then leads the laser light to the sample and de-scans the emission light (green and red), directing it at the pinhole (Pn) where it reaches the detector. b) The pinhole eliminates the out-of-focus light and therefore enables axial sectioning. L= lense 18

Figure 8: Overview of size scales that can be resolved by light, super-resolution and electron microscopy. Super-resolution approaches allow to surpass Abbe's diffraction limit ~250*nm* thereby extending the resolution power in fluorescence microscopy to 40—100*nm*. 20

Figure 9: Amplifying the sample leads to optical separation of molecules. In the expansion process the labeled structures are moving apart from each other and the distances between two marked molecules/receptors increase. The values of d_1, d_2 and d_3 are not based on real data, but arbitrarily chosen. In fourfold expansion the distance increases ~4x times, in tenfold expansion the distance is ~10x times bigger. 22

water. The protocol for 4x and 10x expansion only differs in the hydrogel composition. 23

Figure 11: Low signal retention due to signal dilution. The same number of fluorophores in the unexpanded sample (a) is then distributed in a 64x times bigger volume in fourfold expansion (b) and

a 1000x times bigger volume in tenfold expansion (c) leading to low Signal-to-Noise ratio in the images. 24

Figure 12: Trifunctional anchored antibodies (b) reach more efficient binding to the gel than ordinary antibody (a). In case a the receptors are first labeled, in a second step the linking solution is added but the binding is arbitarly (dashed circle) while for case b the linking molecules are directly attached to the dye (dashed circle). 25

Figure 13: Illustration of colocalization principles with higher number of green signal than red signal (a). M_1 and M_2 give distinctive correlation values, while M_1 has a value of 1, M_2 has a lower value of 0.6 since there is only a lower number of red signal that can overlap (b). M_2 is therefore distorting the “true” colocalization, leading to a lower amount of overlap only due to different numbers of fluorophores. 28

Figure 14: While MOC (or better M1) can handle different fluorescent intensities (c), PCC gives distorted results of fractional overlap of green and red fluorophores. Colocalization (yellow) depends on the degree of overlapped fluorescent signals. For case a) PCC=1, M_1=1 and M_2=1, for case b) PCC=0, M_1=0 and M_2=0 and for case c) PCC=0.5, M_1=1 and M_2=0.25. M_1 gives the most accurate result (c) as the low number of red signal falsely leads to a low coefficient M_2. All numbers are replicate of those calculated by Manders et. al, 1993[101] 28

Figure 15: Image pre-processing. Before analyzing the colocalization in platelets, the receptor distribution of GPIIb/IIIa (either labeled with A488 or A594) in images were preprocessed by chromatic shift correction (A): raw unexpanded platelet, deconvolution (B): raw (upper panel) and deconvolved 4x expanded platelet (lower panel) and thresholding (C): deconvolved (upper panel) and masked surface of 4x expanded platelet (lower panel). Scale bars 3µm. A modified version of this figure was pre-published.[84,85] 40

Figure 16: Experiment design for Colocalization test cases. Same receptor, but different epitopes (condition I), same receptor with the same epitope (condition II) and two different receptors (condition III). 40

Figure 17: Decision tree to validate optimal sample preparation and to choose the appropriate colocalization coefficient. The numbered aspects on which has been focused in the result part are gel diameter, platelet diameter, signal intensity and the number of voxels in expanded, resting platelets. 42

Figure 18: Gel diameter (upper row) and platelet diameter (lower row) of unexpanded (left), 4x expanded (middle) and 10x expanded samples (right). While for the unexpanded samples, gel and platelet diameter do not vary a lot, for 4x expanded samples and 10x expanded samples the distribution is broader. 44

Figure 19: Dual-colour microscopic images of unexpanded (A), four-fold expanded (B) and ten-fold expanded platelet (C). In all three platelets, two different epitopes of receptor GPIIb/IIIa were labeled either with Alexa 488 (green) or Alexa 594 (magenta). Scale bar: 5µm. This figure was pre-

slightly bigger than Hilberg's gel. Scale bar 2 cm 45

Figure 21: Signal intensities of GPIIb antibody 5D7 (left) and 14A3 (middle) conjugated with fluorophore A488 and A594 and GPIX antibody 56F8 conjugated with A594 (right). The dark green bars are showing the signal intensity in 4x samples of A488, the light green bars the signal intensity in 10x samples. For A594 the bars are colored in dark (4x) and bright (10x) magenta. 46

Figure 22: Microscopic images of 10x expanded platelets labeled with 5D7A488(A), 5D7Att488 "trifunctional" (B) and 5D7Att488 "trifunctional" with additional linking solution (C). When looking at the signal intensities in the images, the original mAB (A) is significantly less bighter than the mAB that contains trifunctional linkers (B). By adding additional linking solution to trifunctional mAB, the signal retention is even higher (C). 5D7 is an antibody to visualize the membrane receptor GPIIb/IIIa. Scale bar 3µm. 47

Figure 23: Higher signal retention with trifunctional linked antibodies. Signal intensities of anti-GPIIb/IIIa labeled with A488, anti-GPIIb/IIIa with trifunctional linkers (Atto488) and anti-GPIIb/IIIa with trifunctional linkers (Att488) + additional linking solution. n=30 48

Figure 24: Scatterplots of signal intensities of unexpanded (left panel), 4x (middle panel) and 10x platelets (right panel). For unexpanded and 4x the scatterplots follow a linear line, while in 10x the signal intensities in the two channels are different. The labeled mABs correspond to condition I in **Figure 16**. 48

Figure 25: Differences of N in two channels. N in the red and green channel of unexpanded platelets is quite even (left panel), while in expanded samples N strongly differs in the two channels. The labeled receptors correspond to condition I in **Figure 16**. n=30 49

Figure 26: MOC depends on expansion factor. MOC vs. diameter of unexpanded (circles), 4x expanded (triangles) and 10x expanded (diamonds) resting platelets labeled with anti-GPIIb/IIIa antibodies (5D7) carrying A488 and anti-GPIX antibodies (56F8) carrying A594 (corresponds with condition III in Table 13). Expanded platelets with a diameter below 12µm were excluded from further analysis (marked in red). A modified version of this figure was pre-published.[84,85] 50

Figure 27: Influence of platelet orientation on MOC. MOC of 4x expanded resting platelets labeled with anti-GPIIb/IIIa antibody (5D7) carrying either Alexa488 (green, right panel) or Alexa594 (magenta, right panel). Diagonal orientated platelets show weaker colocalization than horizontal orientated ones and were excluded from further analysis. Scale bar 4µm. A modified version of this figure was pre-published.[84,85] 50

Figure 28: Performance of colocalization test case results based on ExM. Comparing the distributions of the average of MOC of groups of six of unexpanded (left, circles), 4x (middle, triangles) and 10x expanded platelets (right, diamonds) . In unexpanded samples the three cases cannot be distinguished due to lower resolution, while in 4x and 10x samples a clear distinction between condition I and III is shown. n.s.: $p > 0.05$, *: $p \leq 0.05$, **: $p \leq 0.01$, (Kruskal-Wallis ANOVA test), n=30. A modified version of this figure was pre-published.[84,85] 51

List of Tables

Table 1: Spectral properties of fluorophores Alexa488 and Atto488. 33
Table 2: Camera setups 37
Table 3: Image filtering 37
Table 4: Approximate localization of molecules 37
Table 5: Sub-pixel localization of molecules 37
Table 6: Visualization of the results 37
Table 7: Settings for generating distortion matrix 38
Table 8: General parameter of the sampling interval 38
Table 9: Optical parameters 38
Table 10: Advanced optical parameters 38
Table 11: Channel parameters 39
Table 12: Settings for restoration 39
Table 13: Three conditions for colocalization test experiment 40
Table 14: F_{exp} calculated from gel diameter (macroscopic) and platelet diameter (microscopic).. 45
Table 15: Advantages and disadvantages of two different gel recipes. 46
Table 16: Experiment design for comparison between original (I) and trifunctional (II, III) antibody 47
Table 17: Acquisition parameters 59
Table 18: Settings of Argon laser (wavelength of 488nm) 59
Table 19: Settings of HeNe Laser (wavelength of 594nm) 59
Table 20: Shapiro-Wilk Test 60
Table 21: Kruskal-Wallis Test 60

1 Introduction

The function of platelets cannot be overstated as they play a crucial role in thrombus formation which can be both lifesaving (hemostasis) and life-threatening (thrombosis). Additional functions of platelets beyond this main role are wound healing, thrombo-inflammatory processes and tumorigenesis and have been intensively researched for a few decades. While thrombus formation has a positive effect on hemostasis by sealing vascular wounds, the pathological formation of a clot can lead to strokes and/or myocardial infarctions just to name the most severe consequences. To prevent those thrombotic events the development of more specific anti-coagulation and antiplatelet medication is necessary as the currently available drugs often increase the risk of bleeding. To design more specific drugs, it is mandatory to fully understand the platelet activation pathway and elucidate the role of abundant receptors such as GPIIb/IIIa and GPIb-IX-V. Thus, the aim of this thesis is to establish a method that shows interactions, clustering, and reorganization of platelet membrane receptors.

When it comes to imaging platelets, there are two main challenges that must be addressed. First, platelets are very small cells (1—3 µm of diameter) and second, most of the membrane receptors are highly abundant. A recently developed technique called Expansion Microscopy (ExM) could help address this issue. By enlarging the sample physically, receptors are drifting apart from each other, thereby improving the resolution power of a conventional fluorescence microscope. Although this technique sounds promising there are some obstacles such as the variability of the expansion factor, isotropy of the expansion process, as well as low Signal-to-Noise ratio (SNR) in images due to reduced signal retention and signal dilution. To validate the suitability of ExM for examining resting platelets, a workflow for optimal sample preparation was established and colocalization test cases were designed. Colocalization as a quantitative measuring method was chosen because it allows assumptions about how receptors are distributed in a defined area. The combination of dual-color ExM and confocal fluorescence microscopy enables imaging in the nanometer range, observing potential receptor clustering in resting platelets that could explain fast clotting reactions of the thrombotic pathway.

In summary, ExM in combination with fluorescence confocal microscopy is a powerful tool when it comes to image densely packed structures. Combining it with super-resolution approaches makes it even more appealing for biological researchers and could be a starting point for lots of new scientific findings.

1.1 Blood platelets in health and disease

1.1.1 General role of blood platelets

The ability of blood to form a clot to seal vascular injuries highly depends on form and functionality of platelets. Platelets are small, anuclear cells, that are produced in the bone marrow where they are fragmented from megakaryocytes and enter blood circulation as so-called proplatelets. The blood stream generates shear forces that cause the fragmentation of proplatelets into platelets.[1] The average count of platelets is about 1.000.000/µl in mice[2,3] and 150.000-450.000/µl in humans.[4] After 7—10 days aged platelets are degraded by macrophages in spleen, lung and liver.[5]

Resting platelets are oval lens-shaped cells of 1—3 µm in diameter. When the integrity of the vascular endothelium is lost due to injuries, platelets get activated and prevent further bleeding by building a clot. Their activation leads to a reorganization of the cytoskeleton and a morphological shape transformation from a discoid into an irregular sphere with multiple filopodial extensions.[6] These filopodia are sticky and increase the cell surface which makes it easier to interlock with neighboring platelets and form a plug.[7] Apart from those hemostatic defense mechanisms to control blood loss and permit vascular wound healing, platelets are key players in thrombosis,[8] atherosclerosis,[9] neurodegenerative diseases[10] and tumorigenesis[11,12], especially in tumor growth/vascularization[13] and metastases.

The involvement in numerous pathways makes platelets a frequent drug target, especially when it comes to the treatment/prevention of myocardial infarctions or strokes where a pathological thrombus is disturbing the blood supply in coronary or brain arteries that leads to ischemia and necrosis in the area past the occlusion. All of the currently used antiplatelet agents have one eminent downside in common: they not only prevent clot formation but also affect general hemostatic mechanisms which lead to increased risk of bleeding.[14,15] So, the aim is to develop drugs that only inhibit initial platelet adhesion and not the complete hemostatic pathway.[16] For this, the complex signaling pathway of hemostasis has to be fully understood and deciphered.

1.1.2 Platelet adhesion and thrombus formation

Hemostasis is a well-balanced protective mechanism to prevent and stop bleeding. The hemostatic pathway is divided into two parts: primary and secondary hemostasis (**Figure 1**). When the integrity of a blood vessel is lost, the smooth muscle cells of the vascular endothelium immediately react with vasoconstriction which reduces the blood flow in the area around the injury and lead to higher shear rates.

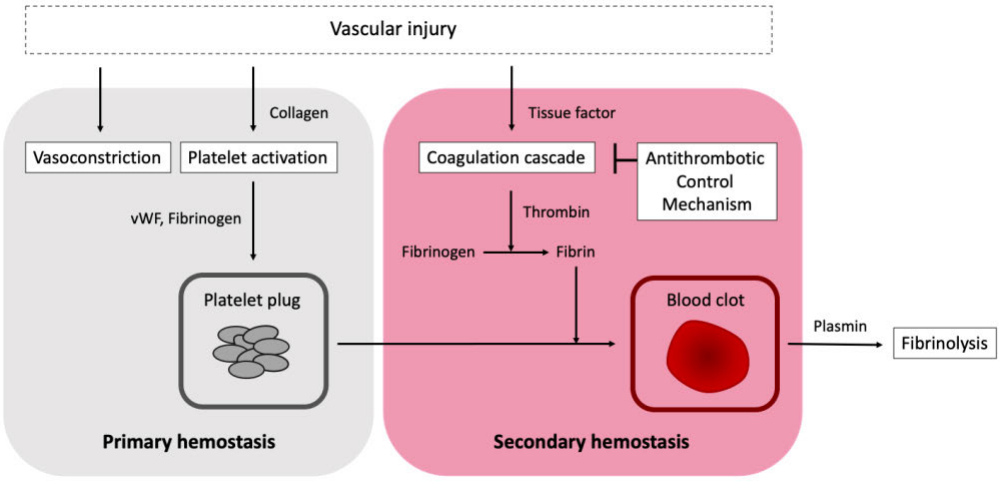

Figure 1: Primary and secondary hemostasis. After sealing the vascular injury with a temporary platelet plug, the coagulation cascade provides a firm and stable thrombus to reconstruct the lesion. After tissue repair, the clot is broken down in a process called fibrinolysis.

Among others, collagen and the glycoprotein von-Willebrand-Factor (vWF) are exposed on the subendothelial matrix of the damaged endothelium.[17,18] Platelets can bind to both vWF and collagen, get activated and form a temporary plug. These mechanisms are part of the primary hemostasis.[19,20] The following secondary hemostasis consists in the sequential activation of clotting factors known as "coagulation cascade" and leads to the formation of a blood clot embedded in a firm fibrin mesh. Beneath this blood clot, the integrity of the injured vascular endothelia is restored. In the course of reconstructing, a serinprotease called Plasmin dissolves the clot by cleaving the meshed fibrin molecules which is referred to as fibrinolysis.[21]

The three most essential membrane receptors for platelet adhesion and activation are the glycoprotein GPIb-IX-V complex, the collagen receptor GPVI and the integrin receptor GPIa/IIa (integrin $\alpha_2\beta_1$)[22], while the receptor complex GPIIa/IIIa is responsible for platelet aggregation.[23]

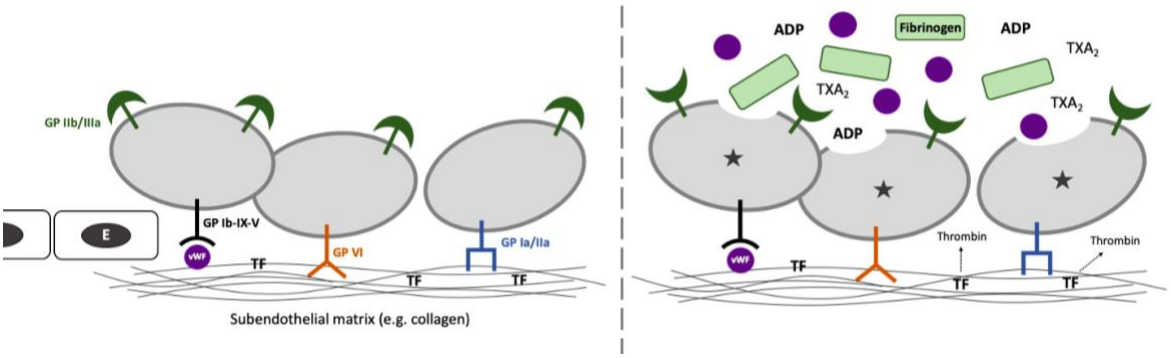

Figure 2: Platelet adhesion (left) and activation (right). GPIb-IX-V first binds to the vWF, GPVI and GPIa/IIa are both binding to collagen. The adhesion of these receptors leads to the activation of platelets (marked by a star) and to a conformational change of GPIIb/IIIa. The secretion of fibrinogen, vWF, ADP and TXA_2 is a crucial part for further platelet activation and aggregation. **E** = Endothelial cell, **vWF** = von-Willebrand-Factor, **TF** = Tissue factor, **TXA_2** = Thrombaxene A_2

The initial tethering of flowing platelets occurs within seconds and is triggered by the binding of the GPIb-IX-V complex to immobilized vWF on exposed collagen (**Figure 2,** left panel). This decelerates the platelets and enables the collagen receptor GPVI to bind its ligand. Ligand binding induces cell activation (marked by a star in Figure 2) which leads to a shift from the resting to the activated state of integrin GPIa/IIa.[7] This process is amplified by locally produced thrombin and the release of fibrinogen and vWF from alpha granules and ADP from dense granules.[24] Activated platelets also generate Thromboxane A_2 (TXA_2) which diffuses through the cell membrane and stimulates further alteration in platelet shape and granule secretion[25] (**Figure 2**, right panel).

Platelet activation also leads to a conformational change in GPIIb/IIIa (integrin $\alpha_{IIb}\beta_3$) from the resting to the activated state. This in turn allows free fibrinogen and vWF to bind to the activated GPIIb/IIIa receptor and serve as bridges between neighboring activated platelets to stabilize the thrombus. As platelet aggregation proceeds, more platelets get activated, generating more secretion so that aggregation increases. This culminates into the formation of a firm, platelet plug that is sealing the wound and prevents blood from penetrating the surrounding tissue (**Figure 3**).[23,6]

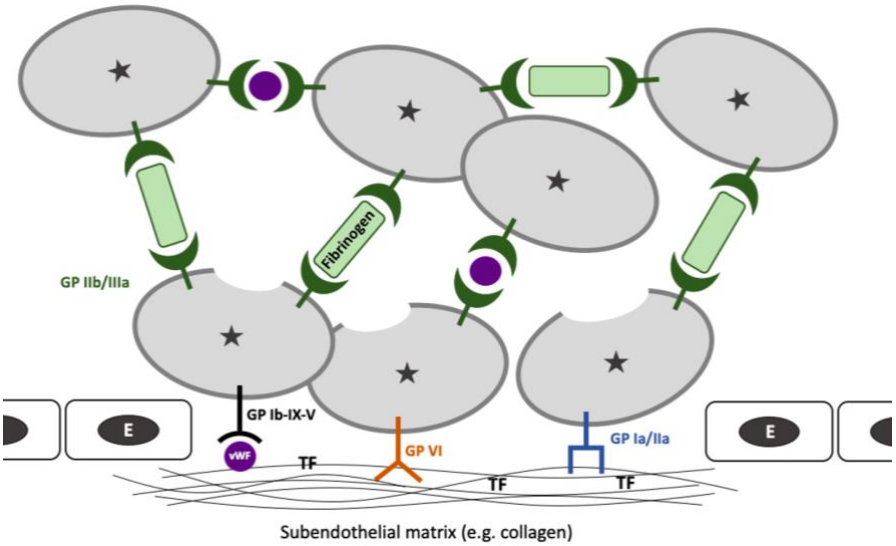

Figure 3: Activated platelet aggregation leads to plug formation. The activation of GPIIb/IIIa enables the binding of vWF and Fibrinogen which function as bridges between activated platelets. The increasing aggregation promotes the formation of a platelet plug which prevents further bleeding. **E** = Endothelial cell, **vWF** = von-Willebrand-Factor, **TF** = Tissue factor, **TXA_2** = Thrombaxene A_2

1.1.3 Platelet receptors

As the membrane glycoprotein receptors GPIb-IX-V and GPIIb/IIIa are the center of the biological questions in this thesis, their specific characteristics will be explained in more detail.

Glycoprotein Ib-IX-V

The organization of the GPIb-IX-V complex is quite unique and consists of four primary polypeptides: GPIbα, GPIbβ, GPIX, and GPV (stoichiometry of 2:4:2:1, respectively). The subunits are either linked via disulfide bridges (GPIbα and GPIbβ)[26], associated tightly, noncovalently (GPIbβ and GPIX)[27] or more loosely (GPV).[28] The major function of this complex is the aforementioned initial tethering of platelets and their activation by binding extracellular ligands such as vWF.[9] These interactions are part of a biochemical signal cascade that lead to the activation of the integrins GPIa/IIb and GPIIb/IIIa, which facilitates stable adhesion and aggregation under conditions of high shear stress.[29] Thereby, the unit GPIbα plays a key role as it not only binds most of the important ligand vWF but also can mediate platelet depletion. After the *in vivo* treatment of mice with anti-GPIbα antibodies (IgG p0p3-5)[30], the platelet counts radically drop and can trigger an Immune Thrombocytopenia in humans.[31] *In vitro,* one anti-GPIbα antibody (92H12) generates so called non-classical clotting, where platelets stick together but do not show their typical activated shape with filopodia (unpublished, **Figure 4**). This phenomenon indicates a functional relevance for dimerization of GPIb-IX-V and raises the question if there might be other signaling pathways apart from the classical agonist-mediated that lead to platelet aggregation. Moreover, dimerization of the GPIb-IX-V complex could induce the re-organization of other membrane glycoproteins, the exposure of adhesive neo-epitopes and/or changes in the cytoskeleton network.[32] However, these processes are not fully understood yet and require further investigation to treat e.g. the Bernard—Soulier syndrome, where the function of GPIb-IX-V is defective.

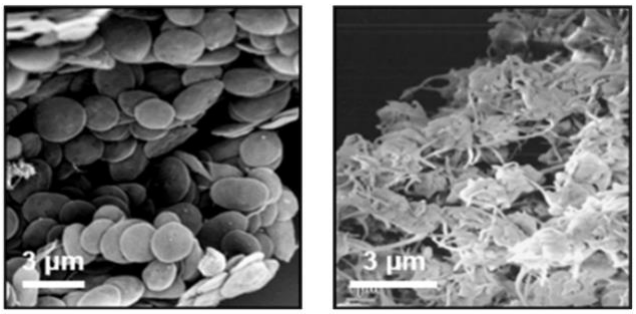

Figure 4: Anti-GPIbα antibody (92H12) induces non-classical clotting. When adding the anti-GPIbα ant body *in vitro*, platelets aggregate (left panel) but do not get activated (right panel). This mechanism is called non-classical clotting. Images with courtesy of Bernhard Nieswandt.

Glycoprotein IIb/IIIa

GPIIb/IIIa, also known as integrin αIIbβ3 or fibrinogen receptor, is a heterodimer compiled from αIIb and β3 monomers in the endoplasmic reticulum. With 120.000 copies it is the most frequent receptor on the platelet membrane[33] and essential for platelet aggregation since it builds cross-links between stimulated adjacent platelets by binding fibrinogen, vWF, fibronectin, vitronectin and fibrin. Before that crosslinking, the GPIIb/IIIa activation is induced almost instantly by agonists such as thrombin and ADP that enable

talin- 1 and kindlin- 3 binding to the β3 domain revealing transmembrane/cytoplasmic domain restraints ("inside-out" signaling).[6] When the synthesis of sufficient correctly folded heterodimers αIIb and β3 is disturbed, the resulting bleeding disorder called Glanzmann thrombasthenia can cause severe damages.[23]

1.2 Visualizing blood platelets down to the molecular level

With the invention of microscopes humanity was able to get a more detailed image of the microscopic world, elevating the resolution power of human eyes from about 0.1 mm to the nanometer scale. This had great impact on scientific discoveries. By using vision as a qualitative tool, we are now able to make assumptions on receptor functions or molecule structures allowing us to understand their complex mechanisms in biochemical processes.

Platelets are very small cells (1—3 µm) riddled with various receptors upon the platelet membrane. Thus, the bottleneck of imaging platelets are their small size and receptor abundance: There are 120.000 copies of GPIIb/IIIa, 35.600 of the GPIb-IX-V complex and 19.700 copies of the GPVI receptor upon each murine platelet membrane, only to name a few.[33] Human platelets have slightly lower copy numbers of receptors.[34] So, even with very high resolution it is difficult to discriminate receptors from one another due to their close proximity. To adequately image platelets with nanoscale precision a different approach is required. One promising method is called Expansion Microscopy (ExM) where the resolution is enhanced by physically expanding the samples so the receptors are positioned much further apart from each other (see chapter 0).

1.2.1 High resolution confocal fluorescence microscopy

a) Principles of fluorescence

One way to visualize platelet receptors is by tagging them with fluorescent markers as this is a convenient way to spot their spatial distribution and dynamics. In 2008, Osamu Shimomura, Martin Chalfie and Roger Tsien won the Nobel prize in chemistry for the discovery and use of GFP (Green Fluorescent Protein) which marks a milestone in multi-color imaging and other applications like spectroscopy or drug discovery.[35,36] Aleksander Jablonski, a polish physicist, depicted the principle of fluorescence in a diagram later named after him (**Figure 5**). The molecule absorbs the incoming light in form of a photon and gets excited from the ground state S_0 to the higher electronic state S_1 which happens within femto-seconds. Although there is not only one transition pathway back to the ground state, the emission spectrum of each relaxation is always transposed to a higher wavelength (= lower energy). When light of an appropriate wavelength excites the fluorescent molecule, it results in a so-called Stoke-shifted light. Because of this characteristic effect, excitation light and fluorescence can be easily differentiated and allow non-invasive studies of function and location of proteins in the specimen.

Despite several advantages over other approaches such as high contrast, high specificity, the use for quantitative analysis and live cell imaging, there are some downsides like photobleaching, quenching and photodamage. These might lead to a degraded contrast and low SNR in the images which reduces the quality of an image.[37]

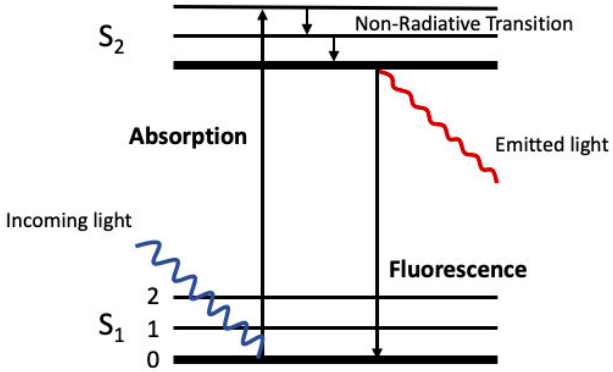

Figure 5: Jablonski diagram shows principle of fluorescence. By excitation of the fluorophore to its excited electronic state S_1 and relaxation to the ground state S_0, fluorescence light will be emitted. The emitted light can then be captured with a sensor or a camera.

b) Principles of light microscopy

For relating to light microscopy and its limitation, the user must be aware of the underlying properties and behaviors of light. Christiaan Huygens, a Dutch microscopist, postulated that light is a disturbance that spreads in all directions as a spherical wave, arguing against Newton´s corpuscular theory. The truth often lies somewhere in between and the agreement on the wave/particle duality of light was announced around 1900 as „neither of them fully explains the phenomena of light, but together they do “, as Albert Einstein stated accurately after having explained the photoelectric effect.[38,39,40]

Refraction

Refraction occurs when a wave changes its direction passing from one medium to another medium. In microscopy these mediums are either air and the glass of the lenses or in immersion, fluid, and glass. When light moves from one medium to another it does not only change direction but also speed, which means that light bends upon changing media. The density of a medium determines the extent of light bending which is called the refractive index (n) and is defined as the speed of light in a vacuum (c) divided by the phase velocity (v):

$$n = \frac{c}{v} \qquad (1)$$

When light hits the lenses, there is a part of light that will be reflected, and some of its information get lost.[41] To decrease the reflection of light in microscopy, the refractive index of two media should be as close together as conceivable.[42]

Diffraction of light limits resolution power

Diffraction is a phenomenon that occurs when a spherical wave front encounters an object and bends around the corners of that obstacle or any aperture such as a pinhole generating new waves and

complex interference patterns.[43] The quality of a lens and thus image quality can be valued by calculating its numerical aperture (NA):

$$NA = n \sin\theta \tag{2}$$

where n is the index of refraction and θ the maximal semi angle of the cone of light that can enter the lens. The consequence is that a high NA results in more narrow fringes at the image plane and can therefore resolve finer details which leads to better resolution. Resolution *d* is defined as the minimum distance at which two points can be observed as two separate points. Over a hundred years ago Ernst Abbe claims that details smaller than approximately one half of the wavelength of light cannot be seen due to the wave nature of light.[44]

$$\boldsymbol{d_{x,y} = \frac{\lambda}{n \sin\theta} = \frac{\lambda}{2 \cdot NA}} \tag{3}$$

$$\boldsymbol{d_z = \frac{2\lambda n}{(2 \cdot NA)^2}} \tag{4}$$

Since light travels in wave front it is not possible that the signal of a point emitter can be focused on an unlimited small spot but rather appears as a broadened distribution called point spread function (PSF). It can be described by a Gaussian function and depends on the wavelength of light λ, the NA of the optical system and the refractive index of the sample medium n[44]:

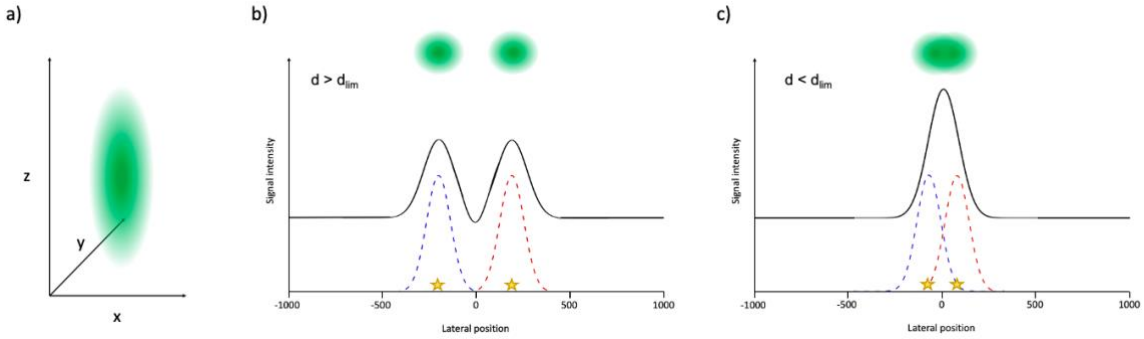

Figure 6: The Point-Spread Function (PSF) and lateral resolution limit of a light microscope. The blurry PSF of a point like emitter is ellipsoid shaped in the axial direction explaining the lower axial resolution (a). PSF widths larger apart from each other than the diffraction limit d_{lim} can be distinguished (b) while objects at a distance below the minimal distance d_{lim} cannot be resolved (c)

Abbe´s equation postulates that the width of the PSF is the shortest distance d_{lim} where two objects can be discriminated (**Figure 6**, b). If the PSFs of two objects are closer together than the distance d_{lim}, the objects cannot be resolved as two separate objects (**Figure 6**, c). In confocal fluorescence microscopy a maximum lateral resolution of ~250*nm* can be achieved, while the axial resolution is limited to ~500*nm*.[45]

Chromatic aberration

Chromatic aberration is the deficiency of optical lenses to focus light rays at the same point (focus) which is caused by the fact that the refractive index depends on the wavelength/color of the light passing through (dispersion). To minimize this contortion achromatic lenses were constructed and aligned in microscopes. The multi-color imaging with a high-resolved fluorescence microscope additionally requires image correction in order to place both color channels exactly on top of each other. [46,47]

c) Confocal scanning microscopy

After introducing the principles of fluorescence and microscopy, the next section deals with a 3D multi-color technique called confocal microscopy. Its composition is built on conventional microscopes where both in-focus light and out-of-focus light was captured which leads to good resolution but generated blurry images. To block out the unnecessary out-of-focus light, a pinhole was inserted, and confocal microscopes entered the stage[48] (**Figure 7**, b).

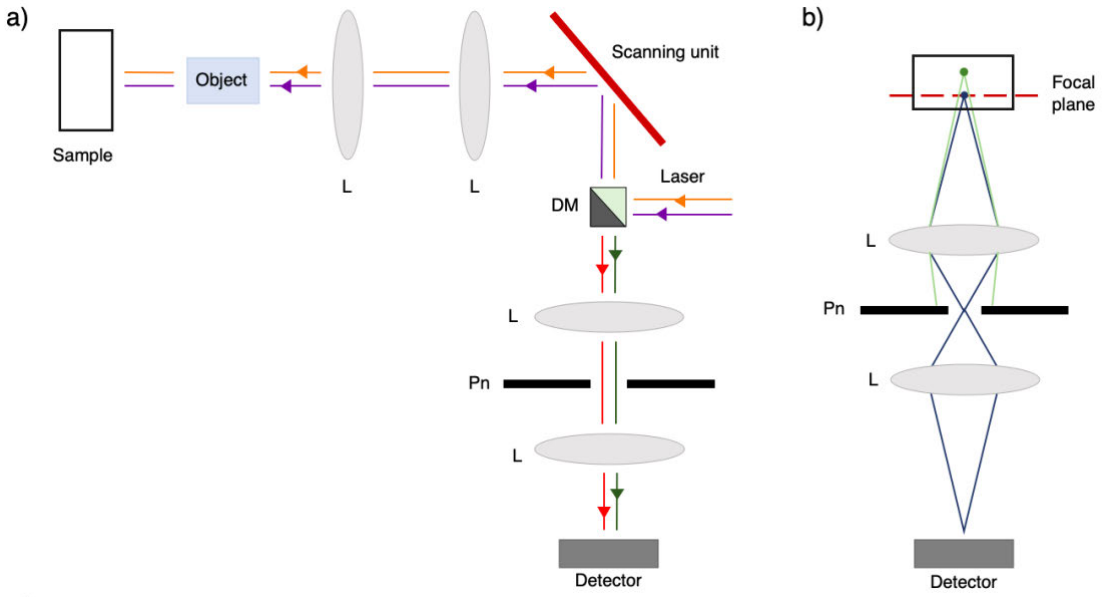

Figure 7: Setup of a fluorescent confocal scanning microscope. a) The excitation lasers (blue and yellow) are directed via a dichroic mirror (DM) towards the scanning unit. The scanning unit then leads the laser light to the sample and de-scans the emission light (green and red), directing it at the pinhole (Pn) where it reaches the detector. b) The pinhole eliminates the out-of-focus light and therefore enables axial sectioning. L= lense

Objective lenses are the core elements of every microscope as they gather light, focus it and add magnification.[49] The distances and angles of lenses and mirrors arranged in an imaging system vary a lot depending on the microscope type. To create an image, scanning mirrors allow to pass over the sample point-by-point registering the intensity at each spot. When mirrors are not being moved, the emitted light will be reflected on the exact same pathway the laser entered the specimen. Because excitation light must be focused to a very limited spot, laser replaced halogen light as they have a high power of collimated light. To separate emitted light from laser light a dichroic mirror (45-degree mirror) is placed in front of the pinhole and emitted light reaches the detector regardless from where it was scanned on the sample (**Figure 7**, a). Detectors are very sensitive photomultiplier tubes which can react within nanoseconds and catch the total amount of light that comes through the pinhole and unlike cameras there is no need to detect the localization of a single spot at a time.[50]

The image acquisition with a scanning device takes time causing difficulties when working with sensitive fluorescent probes. To diminish photobleaching and photodamage the scanning unit could be replaced by a resonant galvanometric mirror that vibrates at a fixed frequency (often at 8kHz).[51] Another drawback is that photomultiplier tubes only record 25% of the arriving photons which makes very dim samples not optimal in confocal microscopy. Using multiple pinholes (Scanning disk confocal) or highly efficient CCD cameras could solve that problem, but they have a limited out-of-focus rejection.[52] After mapping the detected light signals of a sample and constructing an image, a computational process called deconvolution can increase SNR and thus enhance image resolution.[53]

1.2.2 Increasing the resolving power of the microscope: Super-resolution microscopy

Overcoming diffraction in light microscopy was declared to be inconceivable until the beginning of the twenty-first century. In that period of time several scientific groups around the world came up with different techniques commonly referred to as super-resolution microscopy (SRM) or nanoscopy with a resolution power between 40–100*nm* by illuminating fluorescent probes[54] (**Figure 8**). The three most common far-field methods are Structured Illumination Microscopy (SIM), Stimulated Emission Depletion Microscopy (STED) and STORM/PALM/fPALM[55,56,57]. Their functionality as well as their pros and cons will be shortly explained.

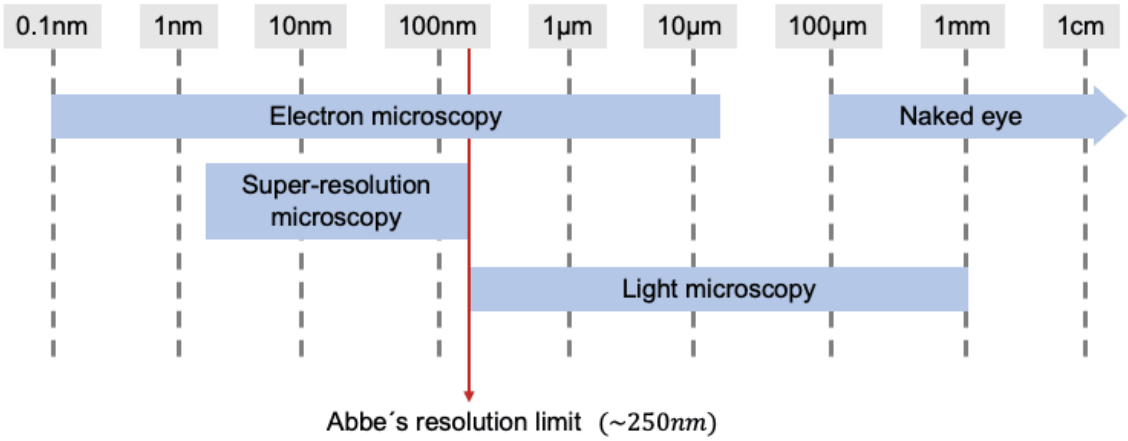

Figure 8: Overview of size scales that can be resolved by light, super-resolution and electron microscopy. Super-resolution approaches allow to surpass Abbe's diffraction limit ~250*nm* thereby extending the resolution power in fluorescence microscopy to 40—100*nm*.

The principle of SIM is that fine structures of an unknown sample are illuminated with striped patterns of high frequency from different angles providing coarse moiré fringes (= interference patterns) that can be transferred to the image plane. For visualizing cell interactions and mechanism standard fluorescent labels and staining protocols can be used[58] making SIM a pleasant technique with a broad range of applications in biology such as visualize mitochondria and tubulin[59] or identify interchromatin channels.[60] Nevertheless, the approach is still improvable as the recording of these multiple patterns requests much stability of the sample and could be accelerated to decrease photodamage.[58,61]

STED is based on fluorescence and was proposed and realized by Stefan Hell and colleagues.[62,63,64] It consists in the controlled depletion of excited fluorophores off the center of the PSF. The depletion beam has a doughnut shape with zero intensity at the center to silence the molecules around the PSF and thereby shape it. The STED light may unintentionally generate fluorescent excitation of the dyes in the depletion region, so suitable dyes must have certain photochemical properties which limits the method compared to conventional microscopy. If the stimulation of the depletion is highly adjusted, the fluorophores close to the inner circle of the doughnut shape center are bleached and cannot emit fluorescence anymore. Although three-color imaging with STED microscopy is still not feasible/difficult due to overlapping excitation and emission of fluorescent markers,[65,66] it has been applied on various

biological probes[67,68,69,70] showing spatial organization of proteins in cells[69] or the extracellular space in living brain tissue.[70]

The idea behind STORM[55]/PALM[56]/fPALM[57] is based on an artistic painting method called pointillism where thousands of dots are added to shape the painting.[71] The problem in conventional microscopy is that the diffraction limited PSFs of particles are overlapping and their localization spot cannot be identified with absolute certainty. By activating a small subset of photoactivatable fluorescent markers at different times with a dim pulse and then illuminate them with excitation light, it is possible to detect the PSF of each fluorophore separately and recalculate the exact localization by defining the center of the fluorescent signal.[72] Their application area in biology is quite diverse yet two-color imaging is most often demonstrated.[73,74,75] Despite the great benefit of this technique, there are still improvements that can be made such as implementing more sensitive detectors/cameras, fasten up the scanning process and develop more sensitive photoswitchable dyes to label not just two cell types but three or four at the same time without increasing phototoxicity.[58]

Platelet receptors are densely packed so not even with super-resolution approaches, receptors can be optically separated from one another. Further drawbacks of SRM are the need of special dyes, slow imaging speed, the difficulty of multicolor 3D imaging and the acquisition of those costly microscopes. A promising, relatively new methodology called Expansion Microscopy (ExM) can be combined with fluorescence confocal microscopy and could solve the major problem of imaging and analyzing high abundant receptors.

1.2.3 Enhancing resolution by amplifying the sample: Expansion microscopy

Unlike any other super-resolution microscopy approach ExM does not rely on a sophisticated optical setup but simply on the physical expansion of the sample itself. Developed in 2015 by a neuroscience lab at the Massachusetts Institute of Technology, ExM allows to enhance the resolution by increasing the sample in size, turning a conventional microscope into a powerful, nanoscale resolving tool (resolution ~25-70*nm*).[76,77]

Basic idea behind ExM

The principle of ExM is based on embedding the sample in a chemically processed cross-linked polymer network (=hydrogel). The dialysis in water, gel, and the linked fluorescence antibodies within it, swell isotropically leading to linear extension of the sample in all three dimensions. The more the optically transparent gel – it mainly consists of water (>99%) – is expanded, the more the labeled structures are drifting apart and can be distinguished from one another (**Figure 9**). The final expansion factor is limited and depends on the monomer composition of the gel.

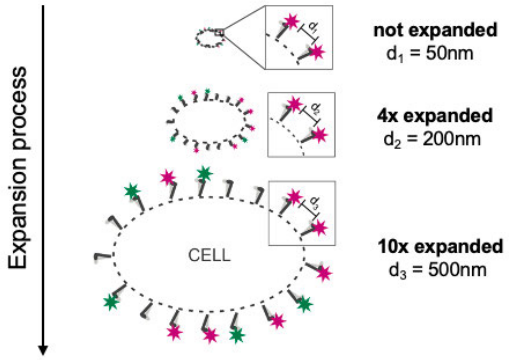

Figure 9: Amplifying the sample leads to optical separation of molecules. In the expansion process the labeled structures are moving apart from each other and the distances between two marked molecules/receptors increase. The values of d_1, d_2 and d_3 are not based on real data, but arbitrarily chosen. In fourfold expansion the distance increases ~4x times, in tenfold expansion the distance is ~10x times bigger.

Expansion protocol adjusted for resting platelets

The original protocol was established for fourfold expansion of brain tissue[76] but labeling strategies and protocol steps constantly have been optimized and modified such as post-denaturation staining[78,79] to diminish signal loss, iterative expansion[80] or tenfold expansion[81,82] where resolutions of 25*nm* can be reached. To apply ExM on resting platelets, the former students Shazeb Ahmad and Max Aigner developed and improved an adjusted 4x expansion protocol[83] based on the first publication of the Boyden Lab. The main credits for this go to MD student Max Aigner who tried out different fixing/linking solutions and tested suitable platelet receptor antibodies for expansion.[84,85] Optimizing tenfold expansion was part of this thesis and consisted in comparing two different 10x gel compositions. The basic expansion protocol always consists of six main steps: fixation of the sample, labeling, linking, gelation, digestion, and expansion. The fourfold and tenfold expansion protocol only differ in the type of polymer composition that was used in the gelation step. **Figure 10** gives a descriptive overview of the protocol steps for resting platelets.

First, platelets are carefully extracted and washed. After fixing them on a coverslip with Glyoxal[86] the targeted receptors are labeled with fluorescent antibodies. The afterwards added linking solution – Acryloyl-X[79] – allows the anchoring of fluorophores to the hydrogel matrix during the polymerization process. The polymer gel for fourfold expansion consists of the monomer sodium chloride, sodium acrylate, the co-monomer acrylamide and the cross-linker N,N`-methylenebisacrylamide. The free radical polymerization is provoked by adding Ammonium persulfate (APS) as initiator and Tetramethylethylenediamine (TEMED) as accelerator.[76] The paper introducing 10x expansion was published by Truckenbrodt et al.[81] The gel polymer matrix for tenfold expansion contains the monomer sodium acrylate and DMMA as cross-linker, the initiator and accelerator of polymerization are potassium persulfate (KPS) and TEMED, respectively.

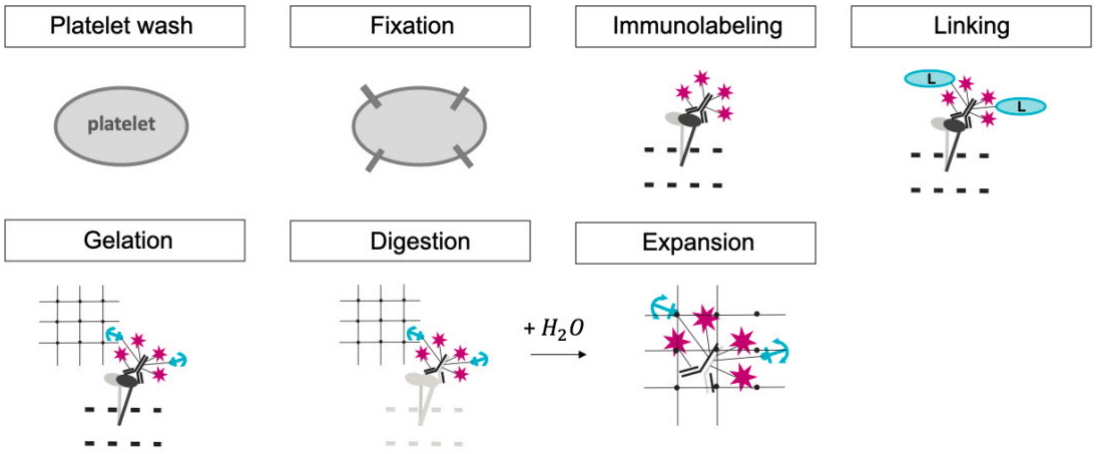

Figure 10: Overview of work steps for either fourfold or tenfold expansion of platelets. After immunolabeling the washed and fixed platelets, the linking solution is added. When gelation is finished, an enzyme digests the cellular components allowing the gel to expand isotropically by adding water. The protocol for 4x and 10x expansion only differs in the hydrogel composition.

In the polymerization process, the acrylamide groups of the linkers attach to the acrylamide groups of the hydrogel building a firm polymerization network (either 4x or 10x). To allow isotropic expansion, the chemical bonds in the sample have to be broken down beforehand, which is achieved through strong, unspecific denaturation using proteinase K.[76] Problems can arise from insufficient protease activity, in which case the platelet membrane stays intact and might cause distortion. Dialysis in fresh deionized water over several washing steps then leads to isotropic gel swallowing where the anchored fluorescent markers within the gel are drifting apart from each other. Even though cell compartments are digested, the fluorophores in the gel are still pinpointing the original localization of the targeted molecules and their position can be imaged with confocal microscopes allowing nanoscale and aberration-free imaging.

4x and 10x gel stability

Both in fourfold and tenfold expansion, the gel diameter increases isotropically in all three dimensions by adding water. The large amount of water (>99%) influences the consistency of gels: the more volume, the less firm the gel becomes. While in 4x expansion the effects on gel stability are relatively small (volume increase of 64x), in 10x expansion (volume increase of 1000x) it can be an obstacle as the handling of the gel and therefore imaging gets more difficult. Against this background, the 10x gel composition developed by Truckenbrodt et al.[81] was compared with an unpublished gel recipe of Tillberg

et al. in order to see if one outperforms the other in view of protocol practicality. For Tillberg´s gel different components were used: sodium acrylate and acrylamide as monomers, N,N′-Methylenebisacrylamide as cross-linker, APS as initiator and TEMED and 4-Hydroxy TEMPO as accelerator.

Signal dilution and fluorophore loss are leading to low Signal-to-noise ratio (SNR)

By expanding linked fluorophores embedded in a polymer composite, the volume of the gel gets 64x times bigger in fourfold expansion and 1000x times bigger by using the tenfold expansion protocol which means that the fluorophore signal drops proportionally to the extent of expansion due to diluted distribution of fluorescent markers (**Figure 11**).

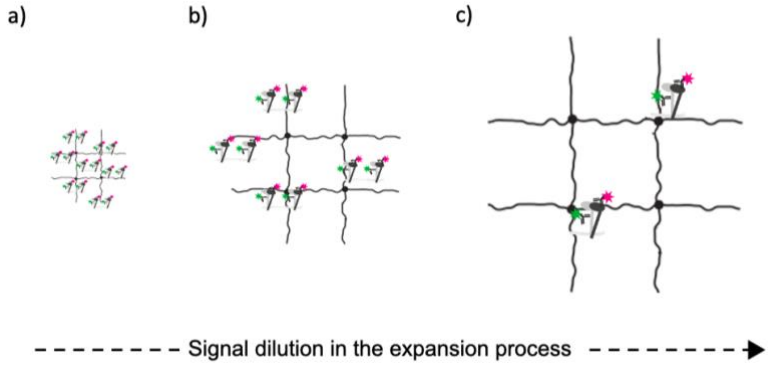

Figure 11: Low signal retention due to signal dilution. The same number of fluorophores in the unexpanded sample (a) is then distributed in a 64x times bigger volume in fourfold expansion (b) and a 1000x times bigger volume in tenfold expansion (c) leading to low Signal-to-Noise ratio in the images.

However, low SNR in expanded images is not only caused by signal dilution but also by simply loosing fluorophores either through inefficient linking or destroyed fluorophores in digestion. According to Shi et al. [87], ~15% of label loss is caused by the polymerization process and ~68% by digestion. The inefficient linking can be explained by the fact that labeling and linking happens in two steps and there is no proof the linker is attached to the fluorophore. If the binding of linkers is arbitrarily and not efficient, fluorophores are not anchored to the gel, thus their fluorescent signal is not captured (**Figure 12**,a).

Likewise, through strong, unspecific protease activity, it cannot be prevented that only cell compartments are digested but also labeled antibody fragments. In general, low signal retention directly effects the quality of images as dim samples are difficult to distinguish from background level. Low SNR of expanded samples can be either increased by higher signal retention or by using another microscope approach with a higher SNR such as Re-scan confocal microscopy.[88]

Reaching higher signal retention with modified antibodies

In the standard expansion protocol, labeling comes first, with the linking solution being added afterwards, the attachment of the chemical linkers (Acryloyl-X) to the antibody does not necessarily imply an attachment to the fluorophore and can be washed out easily (**Figure 12**, a). If the antibody is stained with a dye that already contains the linking molecule (= trifunctional linker), it makes binding more specific and efficient (**Figure 12**, b). The preparation of trivalent anchored antibodies for platelet receptors is based on the publication of Wen et. al.[89] where 2-Iminothiolane is functioning as a chemical

bridge between antibody and dye by attaching thiol- groups to the antibody that are then binding to thiol-groups of the dye (thiol-malemeide chemistry).

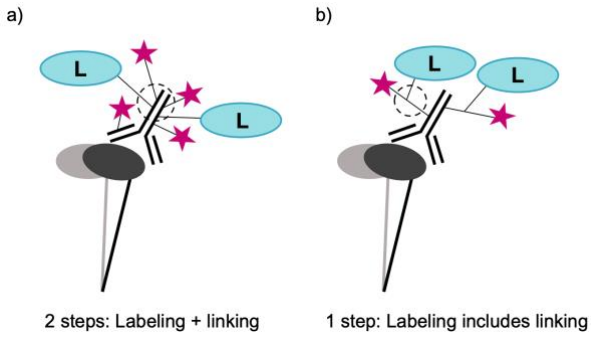

Figure 12: Trifunctional anchored antibodies (b) reach more efficient binding to the gel than ordinary antibody (a). In case a the receptors are first labeled, in a second step the linking solution is added but the binding is arbitrary (dashed circle) while for case b the linking molecules are directly attached to the dye (dashed circle).

ExM in combination with super-resolution microscopy

If the resolution gain of ExM is not sufficient for answering biological questions with certainty, the combination with super-resolution microscopes is a promising method as it allows 3D-multicolor imaging in the nanoscale range like various publications have shown.[90,91,92,93,94,95] The combination of ExM and super-resolution microscopy though is limited by the lower number of suitable fluorophores that makes labeling and linking more elaborate protocol steps.

1.3 Together or single: Colocalization as a key parameter to identify interaction zones in platelets

1.3.1 Colocalization analysis as quantitative statistical measurement of the relationship between two molecules

To analyze receptor distribution and the relationship between them, colocalization analysis was chosen as a quantitative measurement tool. Colocalization in fluorescence microscopy can either be seen as co-occurrence, the statistical spatial pixel-based overlap of two different fluorescent signals or correlation, the statistical spatial overlap and co-distribution of two different fluorescent signals in dependence of one another.[96] Colocalization enables the classification of the degree of physical vicinity and dependence of two molecules allowing assumptions of how they are distributed in a cell or a cell compartment which requires measuring in the three-dimensional space. The variety in shape and complexity of cell structures must be considered as it influences the choice of which colocalization coefficient is the most applicable. The veracity of colocalization analysis highly depends on the resolution of the optical system because the exact physical localization of a molecule in a three-dimensional space is often distorted through the PSF and the wave character of light that leads to an asymmetry in axial and lateral resolution (equation (3) and (4)). So, generating reliable results in colocalization analysis requires good knowledge of the optical system and image acquisition, as well as having an idea of the 3D-organization of the sample and the quality of used labeling markers.[97]

1.3.2 Image acquisition and image pre-processing crucial for colocalization analysis

Correct sampling and intensity levels in images

To avoid under- and oversampling when imaging in three dimensions it is highly recommendable to choose acquisition parameters such as pixel size and z-step depth that are as close as possible to the resolution limit of the microscope. The so-called Nyquist criteria helps microscopists to calculate the appropriate pixel size and is described by 0.3λ/NA. Larger voxels could create artifacts and distort colocalization results, while oversampling beyond the Nyquist frequency leads to prolonged exposure and therefore photobleaching.[98] Also, saturation should be avoided as it leads to information loss of the most intense pixel values.

Circumvent bleed-through and cross-talk

Every fluorochrome has a certain excitation and emission spectra. If more than one fluorophore at a time is labeled, fluorescence can inappropriately pass the neighboring channel generated by an overlap of emission spectra which is known as bleed-through. Cross-talk occurs when two different fluorophores are excited with the same wavelength. For colocalization studies it is essential to choose fluorophores whose emission and excitation spectra can be discriminated precisely to avoid bleed-through and cross-talk.[37]

Deconvolution of images

Every microscopic image in a three-dimensional space is distorted by the composition of multiple blurred PSFs and this distortion is exactly described by a convolution of the objects image with the PSF. The computational process of restoring the original image through sharpening of the PSF is called deconvolution and is critical for colocalization analysis.[99]

1.3.3 Quantifying colocalization based on pixel intensity: Pearson´s correlation coefficient (PCC) and Manders` overlap coefficient (MOC)

To estimate the relationship between fluorophore intensities statistical metrics are used to make assumptions about the correlation or co-occurrence between two molecules.

Pearson´s correlation coefficient (PCC)

In 1896 the mathematician Karl Pearson derived an equation for population studies[100], which Erik Manders applied for the first time to fluorescence microscopy in 1993.[101] PCC already indicates that it belongs to the group of correlation coefficients where the relationship is measured by looking at the signal intensities in the pixels of one image and the corresponding intensities in this pixels in a second image. In summary, PCC is a statistical coefficient that calculates the predictability of the relationship between two random fluorescent signals assuming a linear relationship.[96]

$$PCC = \frac{\Sigma_i (R_i - \bar{R}) \times (G_i - \bar{G})}{\sqrt{\Sigma_i (R_i - R)^2 \times \Sigma_i (G_i - G)^2}} \quad (5)$$

where R_i and G_i refer to the intensity values of the red and green channel of pixel *i.* $\bar{R}$ and $\bar{G}$ indicate the mean intensities of the red and green channel over the entire image. The values of PCC can range between -1 and 1, while 1 indicates a positive correlation (when number of red fluorophores increase at this position, it is likely that the number of green fluorophores increase proportionally), 0 stands for random or independent distribution and -1 suggests a negative correlation (when number of red fluorophores increase at this position, it is likely that the number of green fluorophores decrease proportionally). Although PCC apparently can distinguish between positive and negative correlation, there has been reports that PCC measurements are often biased to the positive which could be solved by using a thresholded PCC[102]. While Pearson´s correlation coefficient is unstable when it comes to diminished SNR, it is less sensitive to redundant low-frequency signal which makes it more robust to fluorescence artifacts. Intermediate values (-0.5 to 0.5) are hard to interpret, which is why PCC is limited to simple settings, also the validity of PCC highly depends on a linear relationship between the red and green pixel intensity. In conclusion, for more complex and nonlinear samples, Manders´ overlap coefficient may be a superior choice.[97]

Manders´ overlap coefficients (MOC)

After introducing PCC to the fluorescence world, Erik Manders developed further coefficients of which the most popular and useful proved to be MOC that determines the total number of pixel-based fluorophores that spatially overlap with each other and thereby measuring the degree of signal co-occurrence. MOC varies from 0 to 1 and can be divided in two separate measurements, M_1 and M_2, that allow accurate colocalization analysis even if the intensities in both channels are different. Unfortunately, MOC is very sensitive to unspecific background signal which is why setting a threshold in image restoration is required to discriminate signal from background. The intensities in the formulas below refer to the intensities over the threshold.[103]

$$M_1 = \frac{\Sigma_i \, R_{i,colocal}}{\Sigma_i \, R_i} \quad (6)$$

where $R_{i,colocal} = R_i$ if $G_i > 0$ and $R_{i,colocal} = 0$ if $G_i = 0$.

In words, M_1 is the defined as the fraction of signal in the red channel which overlaps with nonzero signal in the green channel. M_2 shows the total colocalized green intensities over threshold divided by total green intensities over threshold.

$$M_2 = \frac{\Sigma_i \, G_{i,colocal}}{\Sigma_i \, G_i} \quad (7)$$

where $G_{i,colocal} = G$ if $R_i > 0$ and $G_{i,colocal} = 0$ if $R_i = 0$.

To emphasize the benefit of two separate colocalization metrics, **Figure 13** visualizes that unequal signal intensities need two coefficients to acquire accurate colocalization results. The number of red

fluorescent signal is lower than the number of green signal and while M_1 gives a value of 1, M_2 has a lower value of 0.6 only because of a lower red fraction that can overlap with green which is distorting "true" colocalization.

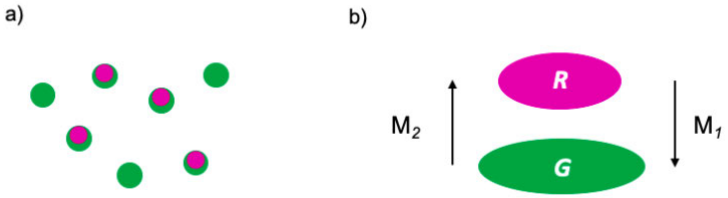

Figure 13: Illustration of colocalization principles with higher number of green signal than red signal (a). M_1 and M_2 give distinctive correlation values, while M_1 has a value of 1, M_2 has a lower value of 0.6 since there is only a lower number of red signal that can overlap (b). M_2 is therefore distorting the "true" colocalization, leading to a lower amount of overlap only due to different numbers of fluorophores.

Figure 14 gives an idea of how colocalization in general can be thought of. The fractional overlap of green fluorophores and red fluorophores is a hundred percent, so PCC, M1 and M2 have a coefficient value of 1 (**Figure 14**,a). For b) in **Figure 14** there is no colocalization at all and the three coefficients have a value of 0. In the third case (**Figure 14**,c) the number of red signal is much lower than the number of green signal. While PCC (0.5) and M2 (0.25) give a value that is lower than 1 because of uneven signal intensities, M_1 has a value of 1 and is therefore not influenced by the lower number of red fluorophores.

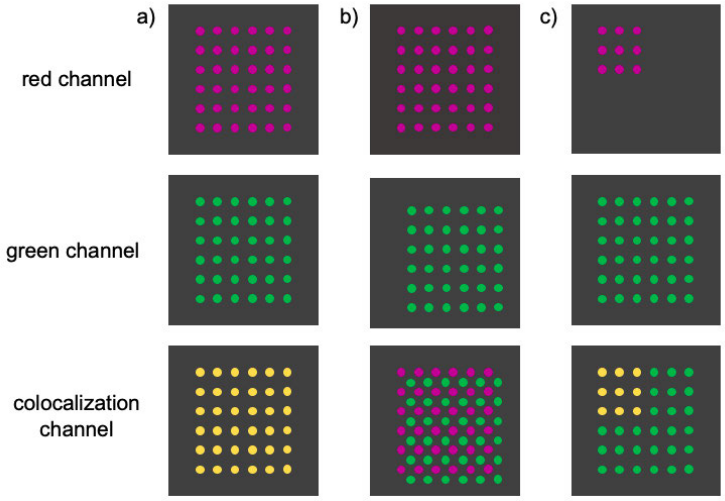

Figure 14: While MOC (or better M1) can handle different fluorescent intensities (c), PCC gives distorted results of fractional overlap of green and red fluorophores. Colocalization (yellow) depends on the degree of overlapped fluorescent signals. For case a) PCC=1, M_1=1 and M_2=1, for case b) PCC=0, M_1=0 and M_2=0 and for case c) PCC=0.5, M_1=1 and M_2=0.25. M_1 gives the most accurate result (c) as the low number of red signal falsely leads to a low coefficient M_2. All numbers are replicate of those calculated by Manders et. al, 1993[101]

In summary, being a direct and more intuitive metric, the MOC has many advantages over the PCC such as its insensitivity to differences in SNR and the ability to look at colocalization from two directions. Still, the use of this coefficient entails image modification if the offset must be identified and excluded. PCC is the preferred method for images if there is no way to determine the background level in each region of interest. For both of them the same difficulty holds true: the differentiation between full and partial correlation is a challenging task and the interpretation of colocalization results is even more demanding.[103]

In this thesis colocalization analysis was used as a tool to study receptor interactions on resting, murine platelets with ExM combined with dual-color confocal microscopy. Here, the main challenge is that expanded samples have a lower SNR than unexpanded ones due to signal dilution in the expansion process and different retention ratios depending on the type of fluorescent marker. So, for a colocalization analysis that does not depend on different marker retention, MOC was chosen. The direction of colocalization always goes from the lower to the higher number of fluorophores as it generates more accurate analysis results. When using this coefficient, one must bear in mind filtering the background in microscopic images which in this case is achieved by image segmentation. The appropriate parameters for the segmentation of expanded platelets were set by Max Aigner.

1.4 Aim of this study

This study aims to develop and validate the approach to map platelet receptor interactions based on the combination of ExM, confocal fluorescence microscopy and colocalization analysis. For this achievement, the 10x expansion process was optimized, modified antibodies were developed, furthermore imaging modalities, image processing and analysis were adjusted. To classify the relationship between receptors as dependent, clustered, or independent, test cases of known maximum and minimum colocalization were designed by using different AB combinations. Based on optimal sample preparation and a clear processing pipeline, the colocalization results of unexpanded, 4x and 10x expanded test case samples were compared to one another and their performance verified and revised. In summary, the study intends to show the limitations and opportunities of colocalization studies on resting, expanded platelets imaged with a confocal fluorescence microscope and to establish ExM as a promising and convenient method in the platelet world.

2 Materials and Methods

2.1 Chemicals and materials

2.1.1 Chemicals and reagents

Reagent	Company
2-Iminothiolane hydrochloride	Sigma (Steinheim, Germany)
4-Hydroxy-TEMPO	Merck (Darmstadt, Germany)
Acrylamide	Sigma (Steinheim, Germany)
Acryloyl-X, SE	Invitrogen (Germany)
Ammonium persulfate (APS)	Roth (Karlsruhe, Germany)
Apyrase	Sigma (Steinheim, Germany)
Bovine Serum Albinum	Roth (Karlsruhe, Germany)
Chloroform	Sigma (Steinheim, Germany)
DMSO	Sigma (Steinheim, Germany)
EDTA	AppliChem (Darmstadt, Germany)
Ethanol	Sigma (Steinheim, Germany)
Fluoroshield™	Sigma (Steinheim, Germany)
Glucose	Sigma (Steinheim, Germany)
Glutaraldehyde	Sigma (Steinheim, Germany)
Glyoxal	Sigma (Steinheim, Germany)
Guanidine HCl	Sigma (Steinheim, Germany)
Heparin	Sigma (Steinheim, Germany)
N,N′-Methylenbisacrylamide	Sigma (Steinheim, Germany)
N,N′-Dimethylacrylamide (DMAA)	Sigma (Steinheim, Germany)
PBS	Life Technologies (Darmstadt, Germany)
Poly-D-Lysin	MP Biomedicals (Santa Ana, USA)
Potassium persulfate (KPS)	Sigma (Steinheim, Germany)
Prostacyclin (PGI_2)	Sigma (Steinheim, Germany)
Proteinase K	ThermoScientific (Roskilde, Denmark)
Sodium Acrylate	Sigma (Steinheim, Germany)
Sodium Chloride (NaCl)	Roth (Karlsruhe, Germany)
Sodium Hydroxid (NaOH)	Roth (Karlsruhe, Germany)
Tetramethylethylenediamine (TEMED)	Roth (Karlsruhe, Germany)
Tris (hydroxymethyl)aminomethane	AppliChem (Darmstadt, Germany)

2.1.2 Materials

Material	Company
Glass coverslip, round (12mm and 24mm)	Marienfeld (Germany)
Heating mat	TRIXIE Heimtierbedarf (Tarp, Germany)
Heparinized capillaries	Hartenstein (Würzburg, Germany)
Microscope slides (24x40mm) #1.5	ThermoScientific (Roskilde, Denmark)
Parafilm	Pechiney (Chicago, IL, USA)
Petridish (round and square)	ThermoScientific (Roskilde, Denmark)
Six-well plate	ThermoScientific (Roskilde, Denmark)
Syringe	Primo (Poland)
Syringe Filter (0.45µm)	Sartorius (Göttingen, Germany)

2.1.3 Gel composition 4x and 10x Expansion

4x Expansion	8.6% Sodium acrylate (w/v), 2.5% Acrylamide (w/v), 0.15% N,N′-Methylenebisacrylamide (w/v), 2 M Sodium chloride, 1x PBS, *added shortly before gelation*: 0.2% TEMED (v/v), 0.2% APS (w/v)
10x Expansion “Truckenbrodt”	2.67% DMAA (w/w), 0.64% Sodium Acrylate (w/w), *added shortly before gelation:* 0.4% TEMED (v/v), 0.4 M KPS
10x Expansion “Tillberg”	11.9% Sodium Acrylate (w/v), 12% Acrylamide (w/v), 0.125% N,N′-Methylenebisacrylamide (w/v), 0.8x PBS, *added shortly before gelation:* 0.16% TEMED (v/v), 0.16% APS (w/v), 0.008% 4-Hydroxy TEMPO (v/v)

2.1.4 Buffers and stock solution

Blocking Buffer	5% BSA (w/v) in 1x PBS
Digestion Buffer	50 mM Tris pH 8.0, 1 mM EDTA pH 8.0, 0.8 M Guanidine HCl. 0.5% Triton X-100 (v/v), *added shortly before use*: 8 Unit/ml Proteinase K
Glyoxal Buffer	19.9% Ethanol (v/v), 7.9% Glyoxal (v/v), 0.76% Acetic Acid (v/v), pH was adjusted to 5 with 2 M NaOH
Tyrode´s Buffer w/o Calcium	137 mM NaCl, 0.43 mM Na_2HPo_4, 2.7 mM KCl, 12 mM $NaHCO_3$, 5 mM HEPES, 1 mM $MgCl_2$, 0.35% BSA (v/v), 0.1% Glucose (w/v)

2.1.5 Antibodies

Antibody	Clone	Isotype	Antigen	Fluorophore	Company/Description
MWReg30	5D7	IgG1	GPIIb	Alexa Fluor 488	[30]
MWReg30	5D7	IgG1	GPIIb	Alexa Fluor 594	[30]
JON6	14A3	IgG2b	αIIbβ3	Alexa Fluor 488	unpublished (B. Nieswandt)
JON6	14A3	IgG2b	αIIbβ3	Alexa Fluor 594	unpublished (B. Nieswandt)
p0p6	56F8	IgG2b	GPIX	Alexa Fluor 594	[104]
self-prepared “trifunctional”	5D7	IgG1	GPIIb	Atto 488	Sophia Maier

* all antibodies were labeled in house

2.2 Methods

2.2.1 Coverslip cleaning

To minimize unwanted background signal during image acquisition the glass coverslips are cleaned for every experiment. The coverslips (Marienfeld Coverslip Ø12mm, #1.5 and Plano Ø24mm) were first sonicated in Chloroform for 1h and dried for a few minutes before they got sonicated in 5M NaOH, again for 1h. Then they get washed several times in ddH_2O until no salt lines were visible and dried with N_2. For storage they were placed in a glass petridish filled with >99% Ethanol.

2.2.2 Coverslip coating

Glycine coating

The coating took place shortly before the platelets had been added to the surface. For every experiment the cleaned and dry coverslips were coated freshly with 2 M Glycine in PBS for 10min at RT. For small coverslips (Ø12mm) 100µl was added, for big coverslips (Ø24mm) 300µl was added. After the washing step, one time with PBS and one time with Tyrode´s Buffer, the coverslips were air-dried.

Poly-D-Lysine coating

The cleaned coverslips (Plano Ø24mm) were coated with 300µl of 0.25mg/ml Poly-D-Lysine for 15min at RT, washed with ddH_2O for 4min and dried with N_2. The coated coverslips were used for fixing the expanded gel pieces during imaging and were prepared just before imaging the samples.

2.2.3 Preparation of antibodies with trifunctional linkers and determination of Degree of Labeling (DOL)

Concentrating antibody solution

For labeling of antibodies with trifunctional linkers, the respective antibodies were concentrated to ~ 2mg/mL using a Vivaspin500 column with a Molecular Weight Cutoff of 10kDa (Polyethersulfon, Neolab), according to the manufacturers' instructions. First the solution was quickly centrifuged at 15.000g to distribute the antibody equally, then put into the Vivaspin500 Column (MWCO 10kDa, Polyethersulfon, Neolab) and centrifuged for 3min at 9.300g. With NanodropOne the concentration was measured assuming an extinction coefficient $\varepsilon_{max}\ (IgG) = 1.37\ L/g \times cm$ per g/mol. Finally, the concentration was adjusted to 2mg/ml with PBS.

Modification of the antibody with trifunctional linkers

The labeling kit was provided by Chrometra (Leuven, Belgium) and contained 1 vial of Activator (5-20 equivalents Iminothiolane), 1 vial of Dye (Att488, around 7nM or 10 equivalents) and 2 purification columns (0.5ml 40kDa Zeba desalting columns, ThermoFisher #87766). To attach thiol groups to the antibody 100µl of the concentrated, unlabeled antibody (2mg/ml) was added to a tube containing 0.4µl 2-Iminothiolane (100mg/ml), mixed thoroughly by vortexing and incubated for 1h at 37°C. The activated antibody solution was then purified with the 0.5ml 40kDaZeba desalting columns spin column at 37°C as described by the manufacturer. Briefly, the purification column was placed into a collection tube and centrifuged for 1min at 1500g. Before adding 300µl of PBS (pH=8), the flow through was discarded. It

was centrifuged again for 1min at 1500g. This step was repeated two more times, the last time instead of 1min for 2min. The column was transferred to a new collection tube, the activated antibody and 15µl PBS were applied on top of the resin to maximize protein recovery and centrifuged for 2min at 1.500g. Before adding the antibody to the dye, it is recommendable to measure the concentration to make sure one has not lost a big amount of antibody. Then, 50µl of the eluted, purified antibody was directly added to the tube containing the reactive dye (Att488, 30:1) solved in 0.5µl DMSO. The reaction took place at 37°C for 1h. For washing out not-reacted fluorophores the labeled antibody was then purified again through spin-column as described above.

Determination of DOL

For the calculation it was necessary to know the concentrations of both fluorophore and antibody. Via measuring an absorption spectrum of AB and fluorescent label with NanodropOne, the concentrations of the labeled AB were calculated. Before measuring, the spectral properties of A488 and Att488 were set manually (Table 1).

Table 1: Spectral properties of fluorophores Alexa488 and Atto488. λ_{max}(absorption)=wavelength of maximal absorption, λ_{max}(emission)=wavelength of maximal emission, cF=correction factor and $\boldsymbol{\varepsilon_{max}}$=extinction coefficient. Spectral properties were taken from respective manufacturer´s websites.

Fluorophore	**λ_{max} (absorption) in [nm]**	**λ_{max} (emission) in [nm]**	**cF**	**ε_{max} in [M-1cm-1]**
A488	496	519	0.11	71 000
Att488	500	520	0.098	90 000

While the concentration of the fluorophores was given in [µM], the concentration of the IgG-antibody was shown in [mg/ml]. For recalculating the concentration, the following formula was used:

$$c(mAB)[\mu M] = \frac{c(mAB)[mg/ml]}{MG\ (IgG)} \times 10^6 \qquad (8)$$

where $MG\ (IgG) = 150´000\ \frac{g}{mol}$.[105]

The DOL of the modified (Att488) and original mAB (A488) was calculated with the following formula:

$$DOL = \frac{c(fluorophore)[\mu M]}{c(mAB)[\mu M]} \qquad (9)$$

2.2.4 Sample preparation

Platelet purification

The acquired ethical permission to do mice experiments was approved by the district government of Lower Franconia (Bezirksregierung Unterfranken). About 1ml murine blood derived from retrobulbar bleeding with heparinized, micro hematocrit capillaries in isoflurane anesthesia was given into tubes (Eppendorf, 1.5ml) filled with 300ml Heparin (20 U/ml Ratiopharm). As Heparin is a strong anticoagulant it diminishes the unintentional activation of the blood platelets. The blood samples were then centrifuged at 800rpm (~300g) for 6min with the Eppendorf Centrifuge 5415C. After transferring the supernatant which contains Platelet Rich Plasma (PRP) into a fresh tube with 300ml Heparin, 5µl PGI_2 (0.1µg/ml, P6188, Sigma-Aldrich) and 2µl Apyrase (0.02 U/ml), the tubes were again centrifuged at 800 rpm for 6min. The supernatant was transferred to fresh tubes containing 300ml Heparin, 5µl PGI_2 and 2µl Apyrase. The subsequent centrifugation at 1500rpm (~800g) for 5min, targeted on sedimenting the platelets, was performed by the Eppendorf Centrifuge 5424. The supernatant was discarded, and the pellet was dissolved in 1ml pre-warmed Tyrode´s Buffer, 5µl PGI_2 and 2µl Apyrase. This step was executed twice. For platelet count measurement 50µl of platelet suspension were mixed with 50µl PBS and placed into the Sysmex KX-21N automated hematology analyzer (Sysmex Corporation, Kobe, Japan) to determine the number of platelets. Only samples with MPV (Mean Platelet Volume) between 5 and 6fl were used. Platelet concentration was adjusted to 300.000/µl by diluting the pellet with the appropriate calculated volume of Tyrode´s buffer and 2µl Apyrase after the third centrifugation at 1500rpm. Platelet suspension was placed in an incubator for 30min at 37°C.

Platelet spreading

Before adding the platelet suspension on glycine coated coverslips (see chapter 2.2.a.) and letting it rest for 20min at 37°C, the platelet concentration had to be adjusted with Tyrode´s Buffer to 150.000 platelets per µl. For unexpanded samples 100µl of platelet suspension was given on each coverslip of 12mm diameter, 300µl of suspension was required to cover the 24mm x 24mm coverslips for the samples, which were used in the expansion experiments.

Fixation and Blocking

To fix the platelets on the coverslip Glyoxal buffer was applied for 2min at 37°C and 18min at RT. Coverslips were then washed 5x times with sterile PBS for 30s, 1min, 5min, 10min and 15min. After washing, the fixed platelets were blocked with 5%BSA for 1h at RT and then washed again 2x times with sterile PBS.

Immunolabeling and preparation of unexpanded samples

The used antibodies had concentrations between 1 and 2.6mg/ml. For the experiment the concentrations were supplemented with 5%BSA (in PBS) to 10µg/ml and added on the coverslips (100µl on 12mm coverslips, 300µl on 24mm coverslips) surface for 30min at 37°C. After immunostaining, the coverslips were washed 5x times with sterile PBS for 30s, 1min, 5min, 10min and 15min.

Preparation of unexpanded samples

The unexpanded control samples were fixed with Glyoxal, mounted with Fluoroshield™ (Sigma) and sealed with clear nail polish on a glass microscope slide (24x25mm).

2.2.5 Preparation of expanded samples

The fourfold and tenfold expansion protocols were quite similar, only the gelation and digestion steps were different.

Linking

After immunolabeling and washing the coverslips, the linking solution Acryloyl-X, SE (0.1mg/ml in PBS) was pipetted onto them and incubated overnight (at least 6h) in a humidified chamber at RT.

a) 4x Expansion

Gelation

The gelation solution was sensitive to any mechanical movements, therefor the handling had to be accurate and careful. For an evenly distributed gel, a plain surface was crucial and achieved by covering the flat backside of a six-well-plate with parafilm. To reduce the speed of the polymer reaction everything was prepared on ice. Before adding the freshly prepared APS and TEMED to the monomer solution it was necessary to first wash off the linking solution (2x times with PBS). When all three components were mixed and vortexed, 50µl of gelation solution were placed on the parafilm for each sample. The coverslips with the platelets were then positioned on top of the drops. The samples should be protected from light and transferred to a humidified chamber. The gelation process took 2h in a 37°C incubator (Memmert, Schwabach, Germany).

Digestion

With great care the coverslip with the solid gel were removed from the parafilm and put into small petri dishes. About 1.5ml of Digestion Buffer plus the added Proteinase K (8 U/ml) were poured to each petri dish covering the gel. The samples were left for 8h at RT in the dark.

b) 10x Expansion

Gelation "Truckenbrodt"

In 10x expansion, the gelation solution was even more sensitive to any mechanical movements, the handling requires great care and accuracy. The monomer solution was bubbled for 40min with N_2 on ice. KPS always had to be prepared directly before use and was then added to the monomer solution to bubble with N_2 for 15min on ice cold water. Before adding TEMED to the gel solution it was necessary to first wash off the linking solution on the coverslips (2x times with PBS). When all three components were mixed and vortexed, 50µl of gelation solution is placed on the parafilm for each sample. The coverslips with the platelets are then positioned on top of the drops. The samples were protected from light and transferred to a humidified chamber. The gelation process only works under low oxygen conditions therefore N_2 is blown into the chamber. After 48h at -4°C the gelation is finished.

Gelation "Tillberg"

The preparation steps were the same as described in *Gelation "Truckenbrodt"*. The reagents and concentrations of the chemicals slightly differed. For preparing the gelation solution, 8.4µl of APS, 8.4µl of TEMED and 8.4µl of 4-Hydroxy TEMPO were added to the monomer solution, vortexed briefly and immediately pipetted onto the parafilm (50µl of gelation solution for each coverslip). The coverslips were then placed on top of the drops and moved to incubator. The gelation reaction was allowed to proceed for 1h at 50°C.

Digestion

After gelation, the coverslips with the firm gel were removed from the parafilm and put into small petri dishes. About 1.5ml of Digestion Buffer plus the shortly before added Proteinase K (8 U/ml) were added to each petri dish covering the gel. The samples were left for 12h at 50°C.

Expansion of 4x or 10x gels by adding water

Through the digestion solution the gels already expanded. For further expansion they were transferred to bigger petri dishes (12x12cm) and covered with 50-70ml of double-distilled water. The water was exchanged 3-5 times a day every 2h and left overnight. When the gels were fully expanded, they were put on millimeter paper and a photo was taken to determine the macroscopic expansion factor. The unexpanded gel was about 1.1cm big. For fourfold expansion a gel diameter of around 4cm was expected, for tenfold expansion a gel diameter of about 10cm. The expansion factor (F_{exp}) was determined by the ratio of unexpanded versus expanded gel diameter.

2.2.6 Imaging unexpanded and expanded platelets

Gel orientation and estimation of expansion factor

Before fixing the cut piece of gel on the coverslip, it was crucial to first check the position of the platelets in the gel. When found, three to five images and one stack were taken, and the diameter of each platelet measured. The approximate diameter showed whether the expansion did work.

Immobilization of gel

During the imaging process a strong attachment of the gel piece on the coverslip was required to avoid movement of the platelets. Therefor the gel´s edges were dried with wipes and then placed on a Poly-D-Lysine coated coverslip.

Microscope setup and Imaging

Imaging was performed on a confocal microscope (Leica TCS SP5) with resonant scanner using the HCX PL APO CS 63.0x1.20 WATER UV objective (Leica Microsystems, Wetzlar, Germany). Images/stacks were acquired in accordance with the Nyquist criteria. For image acquisition settings see Table 17.

2.2.7 Microscope calibration

a) Chromatic aberration correction and channel alignment

Beads

About twenty images of 200 nm TetraSpeck™ (T7279) beads were taken for each channel with the same detector settings and zoom factor as used for imaging the platelets. Differences in laser intensity are insignificant. A median filter with radius 4px was applied to every image in Fiji[106] (ImageJ, National Institutes of Health, Bethesda, MD, USA).

ThunderSTORM

For merging the bead images to one stack, the Fiji plugin ThunderSTORM[107] was used with following settings:

Table 2: Camera setups

Pixel size (nm)	41.01
Photoelectrons per A/D count	3.6
Base level (A/D counts)	0.0
EM gain	not checked

Table 3: Image filtering

Filter	Median Filter
Kernel size (px)	4
Pattern	box

Table 4: Approximate localization of molecules

Method	Local maximum
Peak intensity threshold	80*std (Wave.F1)
Connectivity	8-neighbourhood

Table 5: Sub-pixel localization of molecules

Method	PSF: Integrated Gaussian
Fitting radius (px)	10
Fitting method	Weighted Least squares
Initial sigma (px)	4.0
Multi-emitter fitting analysis	not enable

Table 6: Visualization of the results

Method	Averaged shifted histograms
Magnification	1.0
Update frequency (frames)	50
3D	not checked
Lateral shift	2

Generation of distortion matrix

In order to generate a distortion matrix to align both channels, the Fiji Plugin bUnwarpJ[108] was used. Therefore, all the bead/signal spots in channel 1 were tagged manually with a landmark. The landmarks in channel 2 were then moved to the exact same, corresponding position of channel 1. A macro file was written to apply the distortion matrix to every stack in a*.lif file. For the script see Appendix B.

Table 7: Settings for generating distortion matrix

Registration Mode	Mono
Initial Deformation	Coarse
Final Deformation	Very Fine
Divergence Weight	0.0
Curl Weight	0.0
Landmark Weight	0.4
Image Weight	1.0
Stop Threshold	0.01
Verbose	checked
Save Transformations	checked

b) Deconvolution and Imaris file converter

Deconvolution was performed in batch mode, using Huygens Professional 19.04 (Scientific Volume Imaging, Hilversum, The Netherlands). The output format was *rd3. The setting parameters are noted here:

Table 8: General parameter of the sampling interval

X (nm)	40.083
Y(nm)	40.083
Z (nm)	167.847
T (s)	1.0000

Table 9: Optical parameters

Numerical apertur	1.2
Lens immersion (Water)	1.330
Embedding med. (Water)	1.338

Table 10: Advanced optical parameters

Objective quality	Good
Coverslip position (µm)	0.000
Imaging direction	downward

Table 11: Channel parameters

	Channel 0	**Channel 1**
Microscope type	Confocal	Confocal
Backprojected pinhole (nm)	333	333
Excitation wavelength (nm)	561	488
Emission wavelength (nm)	617	525
Multi photon excitation	1	1
Excitation fill factor	2.00	2.00

Table 12: Settings for restoration

Algorithm:	Classical Maximal Likelihood Estimation
PSF mode:	Theoretical
Max. iterations:	40
Iteration mode:	Optimized
Quality change threshold (%):	0.1
Signal to Noise Ratio:	30
Background mode:	Auto
Background estimation radius:	0.7
Relative background:	0.0
Bleaching correction:	If possible
Brick mode:	Auto
PSFs per brick mode:	Off
PSFs per brick, manual mode:	1
Array detector reduction mode:	Auto

With the Imaris file converter 9.5.0 (Bitplane AG, Zurich, Switzerland) the deconvolved images in r3d-format were transformed into the Imaris file format.

c) Image Analysis with Imaris

After deconvolution of the images, Imaris 9.5.0 (Bitplane AG, Zurich, Switzerland) was used to calculate the colocalization between the two labeled molecular distributions. Before finally the colocalization analysis was performed, several preparation steps were required.

Cropping the platelet

To minimize the background signal to its maximum, the first approach was to crop out the platelet of choice.

Determine microscopic expansion factor

The measurement points were all set in the same z-level. The expansion factor is the expanded diameter divided by the unexpanded diameter.

Creating masked surfaces and export masked channel properties

For generating a surface of each channel, the Surface Module in Imaris 9.5.0 was utilized. The surface implied the required thresholding for colocalization analysis with MOC. The intensity threshold (I_{thresh})

was set to values between 1 and 15 au for unexpanded samples and 2 to 30 au for expanded samples, depending on the quantity of fluorophores. The volume threshold was set to values between 100 and 1000nm. The created surfaces were masked as new channels, their signal intensities (I) and their number of voxels (N) were exported and transferred to a table. **Figure 15** gives an overview of all imaging pre-processing steps. First, chromatic shift correction was performed, then deconvolution and creation of masked surfaces by setting thresholds.

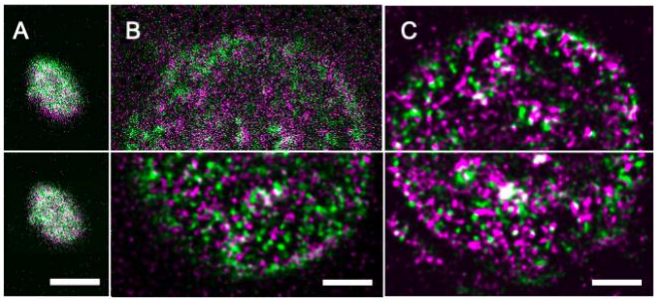

Figure 15: Image pre-processing. Before analyzing the colocalization in platelets, the receptor distribution of GPIIb/IIIa (either labeled with A488 or A594) in images were preprocessed by chromatic shift correction (A): raw unexpanded platelet, deconvolution (B): raw (upper panel) and deconvolved 4x expanded platelet (lower panel) and thresholding (C): deconvolved (upper panel) and masked surface of 4x expanded platelet (lower panel). Scale bars 3µm. A modified version of this figure was pre-published.[84,85]

Quantifying colocalization with MOC (M_1 or M_2) and colocalization test case design

By building a colocalization channel between the two masked channels representing the receptor distribution (intensity threshold was set to 1), the colocalization results were saved, exported, and transferred to a table. The number of voxels (N) of both channels was decisive to see which channel had a greater number of fluorophores. If $N(red) < N(green)$, then M_1 was chosen, while for $N(green) < N(red)$, M_2 is the more appropriate coefficient. For further understanding see chapter 1.3.3 To approve the practicality of ExM and confocal microscopy combined with colocalization analysis, test cases were designed (Table 13). By using different antibody combinations that are known for either high, clustered, or low colocalization, receptor interactions can be analyzed (**Figure 16**).

Table 13: Three conditions for colocalization test experiment

Condition	Receptor	Epitope	Receptor	Epitope	expected Colocalization
I	GPIIb/IIIa	a	GPIIb/IIIa	b	high
II	GPIIb/IIIa	a	GPIIb/IIIa	a	clustered
III	GPIIb/IIIa	b	GPIX	-	low

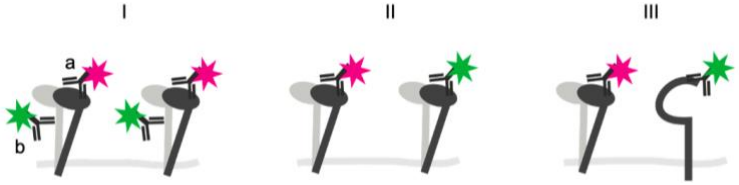

Figure 16: Experiment design for Colocalization test cases. Same receptor, but different epitopes (condition I), same receptor with the same epitope (condition II) and two different receptors (condition III).

Calculation of signal intensity in expanded platelets

The comparison of the signal intensities between 4x and 10x expanded platelets was relatively easy as the exact same imaging parameters were set. For this, the signal intensity (*I)* in a platelet had to be calculated using the following formula:

$$I = S - (I_{\text{thresh}} \cdot N) \quad (10)$$

where S is the (measured) signal.

d) Statistical Analysis

Statistical analysis was performed using Origin 2019 (OriginLab Corporation, Northhampton, United States). We tested for normal distribution using the Shapiro-Wilk test (see Table 20). According to the normality results, the Kruskal—Wallis test was chosen to prove the null - hypothesis: {The samples come from the same population} (see Table 21). Significance level was set to 0.05.

2.2.8 Guideline of sample preparation and colocalization analysis of resting, expanded platelets

Expanding a sample is a challenging task in which a lot of factors arr involved. For our purposes the platelets are imaged in the resting state as it was a known system that serves as control group for colocalization analysis. Once the resting platelets are placed into the gel, the expansion process begins by adding water and continues by exchanging the water every three hours for one and a half day. The success is visible as the gel size increases. Measuring the gel diameter is therefore one of two indicators for a successful expansion process (**Figure 17**,1.) If the gel does not expand, further troubleshooting in gel preparation and/or expansion steps is required (**Figure 17**,2.). The second indicator for a successful expansion process and perhaps the more important one is the diameter of the expanded platelet (**Figure 17**,1.). If the platelet diameter is not four- or tenfold bigger, then digestion has not worked as expected and required. To allow isotropic expansion, the molecular bonds in the sample must cut first, which is achieved by adding proteinase K, a strong and unspecific enzyme. Problems can arise from insufficient protease activity, in which case the platelet membrane remains intact and therefore cannot expand.

Another significant criterion is the achieved signal intensity. In expanded platelets the signal is lower than in unexpanded ones, the reasons for that and possible solutions are listed in chapter 1.2.3 (**Figure 17**,3. and 4.). If the signal is very low, the sample is not valid and should just been used to set up a hypothesis and not for underlying an argument. When sample preparation is approved, the analysis part begins. The principles of Colocalization analysis are explained in further detail in chapter 1.3.3 therefore it will be only referred to the main statements. The next step to take is evaluating the scatterplots of signal intensity data for linearity. If there is a linear relationship, PCC can be used otherwise MOC is the preferable coefficient. For MOC measurements it is important to calculate the number of voxels N in a platelet to decide whether M1 or M2 should be used for interpretations (**Figure 17**,5.). If N in the red channel is lower than in the green channel, M1 is the appropriate choice. M2 is more suitable for the case vice versa. The reasons for this proceeding are described in chapter 1.3.3. In case that N significantly differ, the outcome is not reliable and should be treated with caution. Colocalization analysis is then presented in plots comparing the test case coefficient values of unexpanded, 4x and 10x expanded platelets. This overview should give a clear orientation of the issues that are presented in the following result part.

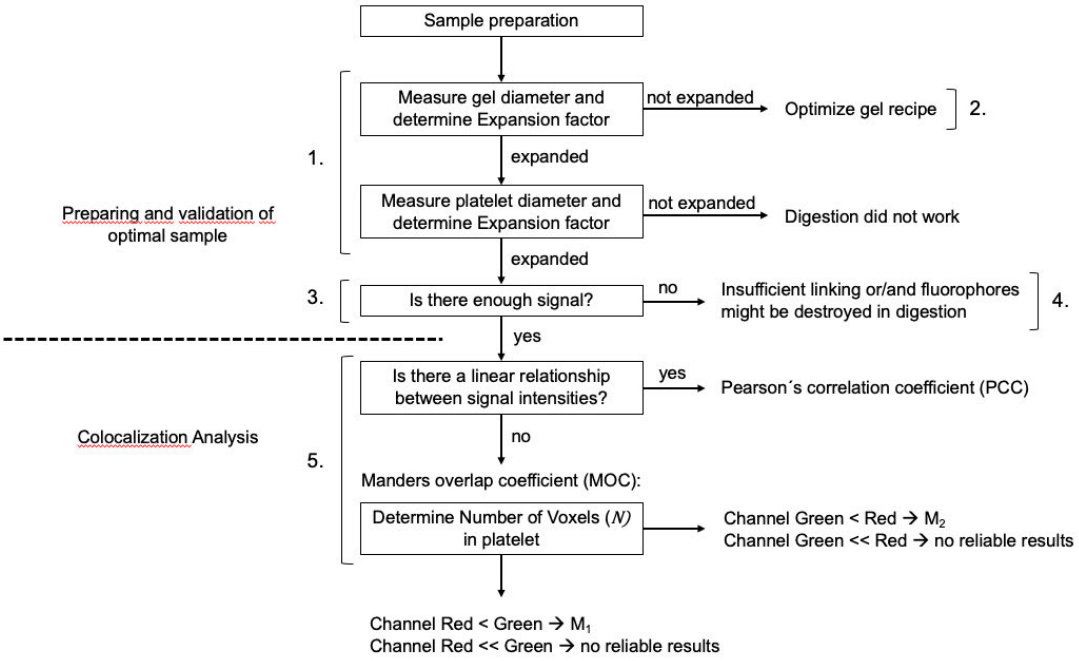

Figure 17: Decision tree to validate optimal sample preparation and to choose the appropriate colocalization coefficient. The numbered aspects on which has been focused in the result part are gel diameter, platelet diameter, signal intensity and the number of voxels in expanded, resting platelets.

3 Results

The general aim of this study is to establish a reliable approach that allows mapping platelet receptor interactions. Imaging of expanded platelets is approached with confocal fluorescence microscopy, as a quantitative measurement for receptor distribution colocalization analysis has been chosen.

ExM is a complex and sensitive process that suffers from low signal retention mostly due to signal dilution. So, the first part of this work includes the optimization of the 10x expansion protocol – the 4x expansion protocol for platelets has been modified by Max Aigner – regarding sample preparation and its reproducibility as well as the preparation and verification of modified, 'trifunctional' antibodies for better signal retention and therefore higher image quality.

To validate the combination of ExM and colocalization analysis, test cases have been designed by using different antibody combinations that are known for either maximum or minimum colocalization and thus provide information about receptor interactions. Based on optimal sample preparation, the precision of colocalization results has been increased by showing the superiority of MOC as colocalization coefficient and the impact of expanded platelet diameter and their orientation. By only including suitable samples, performance, and dynamic range of high and low colocalization test cases are compared in unexpanded, 4x and 10x expanded, resting platelets. The results regarding each aspect are described in detail in the following sections.

3.1 Optimized sample preparation

3.1.1 Experimental expansion factor and reproducibility

For determining the expansion factor there are two references that can be used: gel and platelet diameter, whereby the last one is the more relevant. For measuring the gel diameter, graph paper is used, and a photograph is taken from which the diameter can be read off. The accuracy of this method for expansion factor determination is limited by defects in the gel or non-circular shape. For the unexpanded gel the mean is about 1.1 cm, for the 4x gel it is 5.3 ± 0.6 cm (n=16) and the 10x gel diameter is around 10.8 ± 1.4 cm (n=17) in average. The platelet diameter is set with the measuring tool in Imaris 9.5.0. Two lines perpendicular to each other are drawn whereas just the longer one is listed. The mean of unexpanded platelet diameter is 3.2 ± 0.4 µm (n=180), 4x platelets are 13.3 ± 3.7 µm in average and the mean of 10x platelets is 22.4 ± 4.9 µm (n=192) (**Figure 18**). One concern might be that taking the diameter is not as accurate as the volume, but comparison has shown that indeed there are not a great difference between those two.

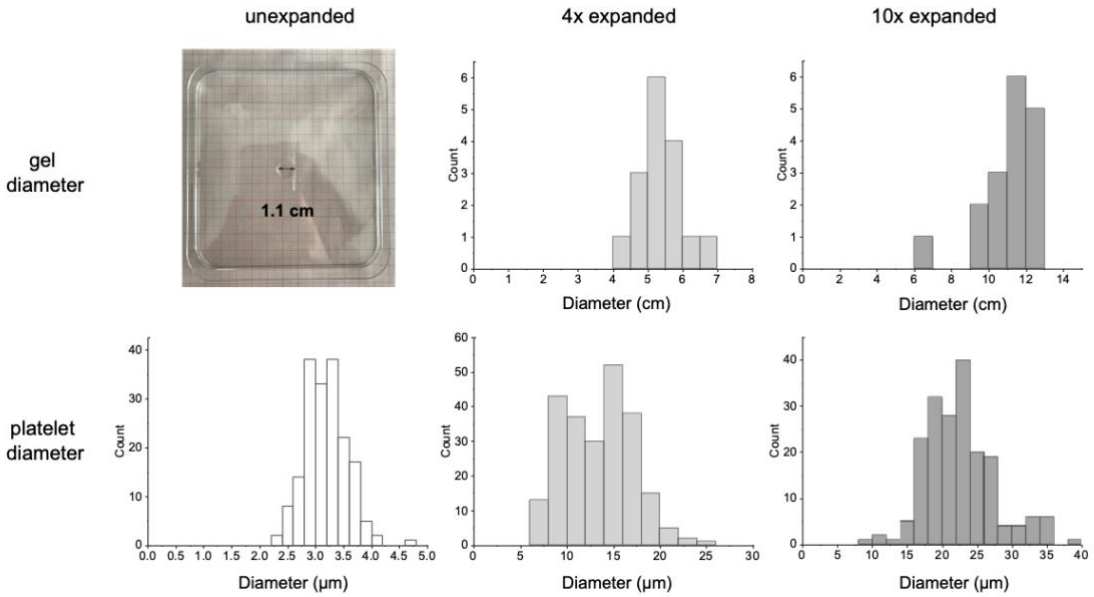

Figure 18: Gel diameter (upper row) and platelet diameter (lower row) of unexpanded (left), 4x expanded (middle) and 10x expanded samples (right). While for the unexpanded samples, gel and platelet diameter do not vary a lot, for 4x expanded samples and 10x expanded samples the distribution is broader.

Figure 19 shows the expansion process of platelets on a microscopic level. The green signal refers to the number of the membrane receptor GPIIb/IIIa, the magenta signal also visualizes the distribution of the receptor GPIIb/IIIa but labeled for a different epitope (Table 13, Condition I). The diminished signal retention throughout the expansion process and uneven proportions of signal intensities in the two channels are noticeable.[84,85]

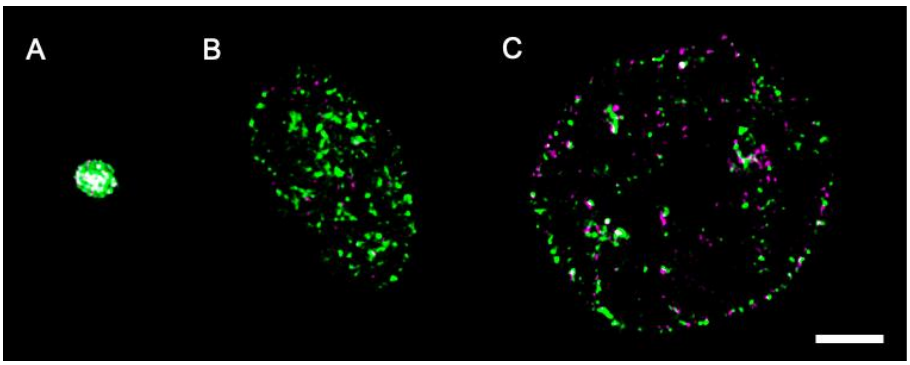

Figure 19: Dual-colour microscopic images of unexpanded (A), four-fold expanded (B) and ten-fold expanded platelet (C). In all three platelets, two different epitopes of receptor GPIIb/IIIa were labeled either with Alexa 488 (green) or Alexa 594 (magenta). Scale bar: 5µm. This figure has been pre-published.[84,85]

For both 4x and 10x expansion the two experiments are listed separately. The macroscopic expansion factor refers to the gel diameter, the microscopic expansion factor is calculated from platelet diameters. The macroscopic F_{exp} in 4x are 3.8 ± 0.1 and 5.1 ± 0.1, for 10x the macroscopic F_{exp} are 8.6 ± 0.6 and 9.8 ± 0.3. For 4x experiment, the microscopic F_{exp} are 3.6 ± 0.5 and 4.9 ± 0.4, while in 10x the microscopic F_{exp} are 7.6 ± 0.4 and 6.4 ± 0.5 (Table 14). The variation of the expansion factor of platelets in two equally approached experiments shows that even if the parameters of the protocol hasn't been changed, the outcome is still quite different. Furthermore, the value of the unexpanded diameter can

bias the results by favoring the big unexpanded platelets over smaller ones. As the microscopic F_{exp} for 4x and 10x varies widely, platelets that have a diameter less than 12µm are not included in the further colocalization analysis to minimize resolution bias and colocalization result distortion.

Table 14: F_{exp} calculated from gel diameter (macroscopic) and platelet diameter (microscopic). The two values in one cell represent two independent repetitions.

F_{exp}	4x	10x
macroscopic	3.8 ± 0.1 and 5.1 ± 0.1	8.6 ± 0.6 and 9.8 ± 0.3
microscopic	3.6 ± 0.5 and 4.9 ± 0.4	7.6 ± 0.4 and 6.4 ± 0.5

3.1.2 10x expansion: Optimized gel protocol

In 10x expansion, gels are mucoid and not very stable, thus the handling of small gel pieces that are necessary for imaging, is challenging. To improve gel stability, apart from the protocol of Truckenbrodt et al., a second gel recipe has been tried out (Tillberg et al., unpublished). The comparison does not result in a clear winner (Table 15). Both recipes are working and depending on the set priorities, one is more recommendable than the other. Using Truckenbrodt´s recipe the gel gets relatively big and thick, but duration takes more than 48 hours, and the platelet diameter is slightly smaller compared to Tillberg´s unpublished gel composition. In the protocol developed by Tillberg et al., the gelation step takes 1h and yields on average larger microscopic F_{exp} but smaller macroscopic F_{exp} and more fragile gels (**Figure 20**). Tillberg´s recipe has been tested just once, Truckenbrodt´s on the other hand twice. Nevertheless, one should always bear in mind that these observations are not cast in stone and that adjustments might shift the advantages and disadvantages towards one protocol.

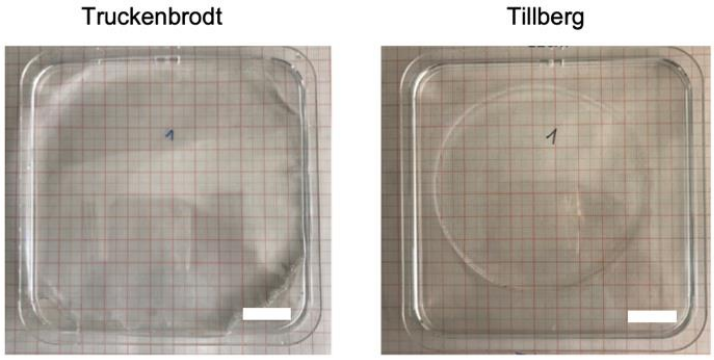

Figure 20: Photographs of Truckenbrodt´s (left) and Tillberg´s gel (right). Truckenbrodt´s gel is slightly bigger than Tillberg´s gel. Scale bar 2 cm

Table 15: Advantages and disadvantages of two different gel recipes. It depends on the focus one sets which recipe is considered the more reasonable.

	Truckenbrodt et. al	Tillberg (unpublished)
Duration of gelation	> 48h	1h
Gel qualities	thick, firm	thin, not so robust
Macroscopic F_{exp}	9.8 ± 0.3	8.6 ± 0.8
Microscopic F_{exp}	6.4 ± 0.5	7.6 ± 0.4
Reliability	two experiments, n=6-12	one experiment, n=3-6

3.1.3 Comparison of the signal intensities in 4x and 10x expanded platelets

As mentioned before there are three reasons that lead to lower signal in expanded samples. The inevitable signal dilution, inefficient linking and/or fluorophore destruction in digestion. The quantitative evaluation between unexpanded and expanded samples is feasible but time-consuming because the imaging settings vary (see Table 18 and Table 19) and a confocal laser-scanning microscopy approach has been applied.[84,85] The signal intensities of 4x and 10x expanded platelets are calculated using equation (10). For the colocalization test experiment (Table 13) three monoclonal antibodies (mAbs) are used: 5D7 and 14A3, which are mABs for the receptor GPIIb/IIIa and 56F8, which is a mAB for receptor GPIX. The first two ones are used either labeled with fluorophore A488 or A594. 56F8 only is required with fluorophore A594. For 5D7A488 the 10x samples show a higher signal retention than 4x samples by the factor 1.4x±0.05 and also for 5D7A594, 10x platelets show higher signal retention than 4x samples by the factor 2.3x±0.7. For 14A3A488 the signal intensity in 10x samples is higher than in 4x by the factor 1.8x±0.02 while for 14A3A594 the signal retention of 4x samples is higher than in 10x by the factor 3.4x±0.2.

For 56F8A594 the 4x samples show a higher signal retention than 10x samples by the factor 7.4x±3.4 (**Figure 21**). The rise and fall of signal intensities in 4x and 10x samples depending on the antibody/dye constellation can be explained by different chemical reactions during digestion in 4x and 10x expansion.

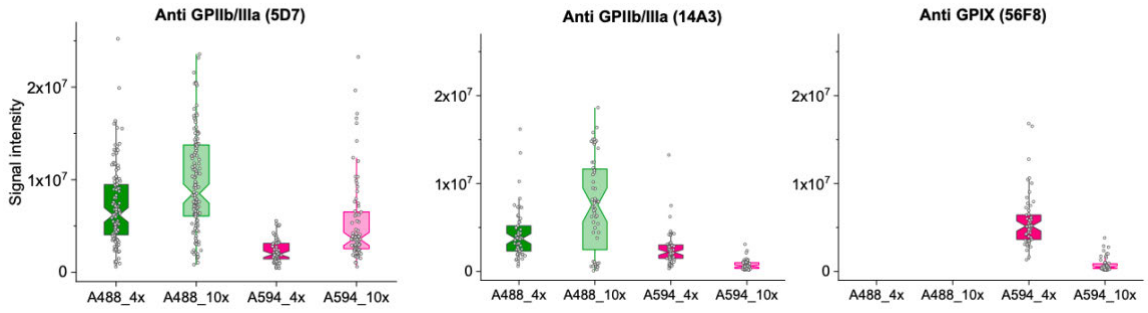

Figure 21: Signal intensities of GPIIb antibody 5D7 (left) and 14A3 (middle) conjugated with fluorophore A488 and A594 and GPIX antibody 56F8 conjugated with A594 (right). The dark green bars are showing the signal intensity in 4x samples of A488, the light green bars the signal intensity in 10x samples. For A594 the bars are colored in dark (4x) and bright (10x) magenta.

3.1.4 Maximizing signal retention by modified antibodies

The use of trifunctional labeled antibodies for expansion microscopy might increase the chance to retain more signal to get images with higher quality. To prove this statement an experiment has been designed where the signal intensity of 5D7A488 ("original" antibody) and the trifunctional linked antibody 5D7Att488 are compared to each other. Further, there has been inserted a third condition, where the linking solution Acryloyl-X is additionally given to the "trifunctional" antibody (Table 16). The DOL of 5D7 conjugated with A488 is 4.8, the DOL of 5D7Att488 is 1.9. For calculating the DOL see equation (9).

Table 16: Experiment design for comparison between original (I) and trifunctional (II, III) antibody

Condition	Receptor	Fluorophore	Trifunctional linkers	Acryloyl-X	DOL
I	GPIIb/IIIa	A488	no	yes	4.8
II	GPIIb/IIIa	Att488	yes	no	1.9
III	GPIIb/IIIa	Att488	yes	yes	1.9

In this experiment the macroscopic F_{exp} is 10.1± 0.4, the microscopic F_{exp} is 9.1±0.6. A different argon laser intensity is used for the trifunctional labeled platelets: the original laser power for expanded platelets is 0.23mW compared to only 12.4µW which are required for the trifunctional samples so that the probes are not sated.

The qualitative difference in signal intensity is already apparent when looking at the microscopic images (**Figure 22**). The 10x expanded platelets stained with the trifunctional linked mAB are much brighter than the platelets where the original antibody has been used.

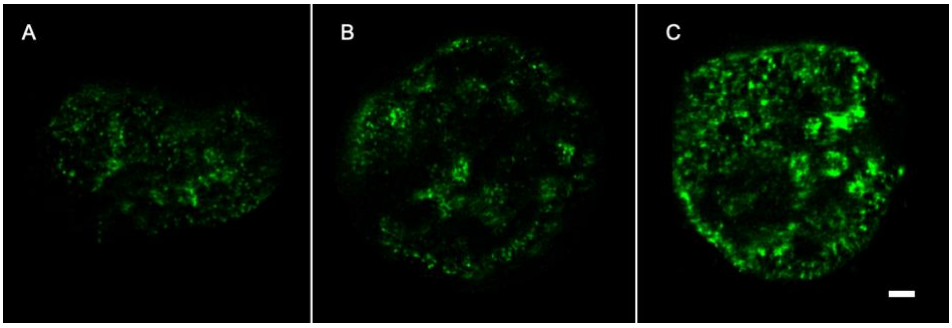

Figure 22: Microscopic images of 10x expanded platelets labeled with 5D7A488(A), 5D7Att488 "trifunctional" (B) and 5D7Att488 "trifunctional" with additional linking solution (C). When looking at the signal intensities in the images, the original mAB (A) is significantly less brighter than the mAB that contains trifunctional linkers (B). By adding additional linking solution to trifunctional mAB, the signal retention is even higher (C). 5D7 is an antibody to visualize the membrane receptor GPIIb/IIIa. Scale bar 3µm.

The benefit of using antibodies that are labeled with trifunctional dyes instead of ordinary antibodies, where the linking solution is added afterwards becomes even more clear when looking at the quantitative analysis presented in **Figure 23**. The plotted bars show the signal intensity calculated for a theoretical DOL of 1 (each mAB is only labeled with one fluorophore), the laser intensity of image acquisition is not considered. The signal intensity of the original mAB ($3.7\pm1.4x10^6$) is significantly lower than the mean value of a trifunctional mAB ($2.3\pm0.9x10^7$) by a factor of ~6.

When adding additional linking solution to the trifunctional mAB, the signal retention is ~14x times higher than the original and ~2x times higher than just the trifunctional mAB ($5.2\pm2.2x10^7$).

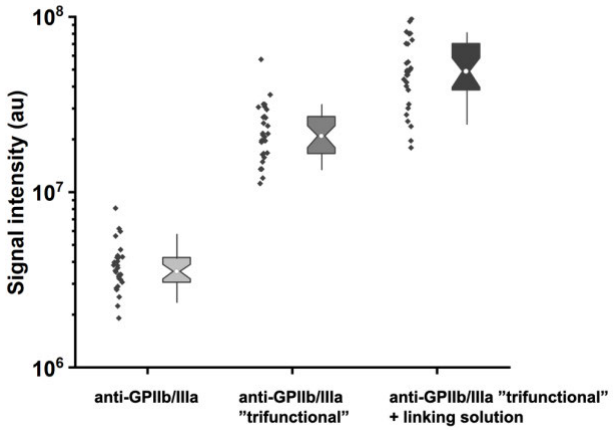

Figure 23: Higher signal retention with trifunctional linked antibodies. Signal intensities of anti-GPIIb/IIIa labeled with A488, anti-GPIIb/IIIa with trifunctional linkers (Atto488) and anti-GPIIb/IIIa with trifunctional linkers (Att488) + additional linking solution. n=30

3.2 Increase of colocalization analysis precision and comparison of colocalization test cases in unexpanded, 4x and 10x expanded resting platelets

3.2 1 Plot ing the pixel signal intensities to look for linearity and determination of of number of voxels (*N)* in platelets

PCC is only applicable if there is a linear relationship between two fluorescent signals. When looking at the scatterplots of unexpanded, 4x and 10x platelets, only one of them shows the required linearity (**Figure 24**, left panel). In 4x and 10x expanded platelets (**Figure 24**, middle and right panel) the signal intensities are generally lower and more spread. Moreover, the red channel demonstrates less pixel intensity than the green channel, wherefore the use of MOC is the preferred measurement method to quantify colocalization in expanded samples (see chapter 1.3.3).[84,85]

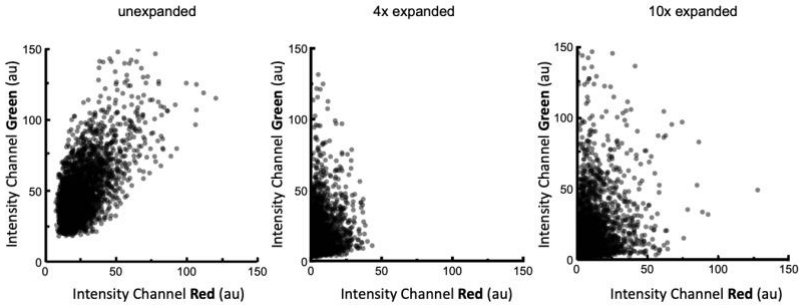

Figure 24: Scatterplots of signal intensities of unexpanded (left panel), 4x (middle panel) and 10x platelets (right panel). For unexpanded and 4x the scatterplots follow a linear line, while in 10x the signal intensities in the two channels are different. The labeled mABs correspond to condition I in **Figure 16**.

The decision which MOC – M_1 and M_2 – is more suitable, depends on the number of voxels (*N)* in each channel. For every case and every expansion level the decision is made individually. **Figure 25** gives an example of how N changes for unexpanded, fourfold, and tenfold examples. While the number of

nonzero-intensity voxels is relatively homogeneous in unexpanded platelets, it varies strongly in expanded platelets. When *N* in the red channel (= Channel 1) is lower than *N* in the green channel (= Channel 2), M_1 is picked. For the reverse situation, M_2 is the more appropriate choice. The reason for this selection is explained in the introduction part (see chapter 1.3.3).

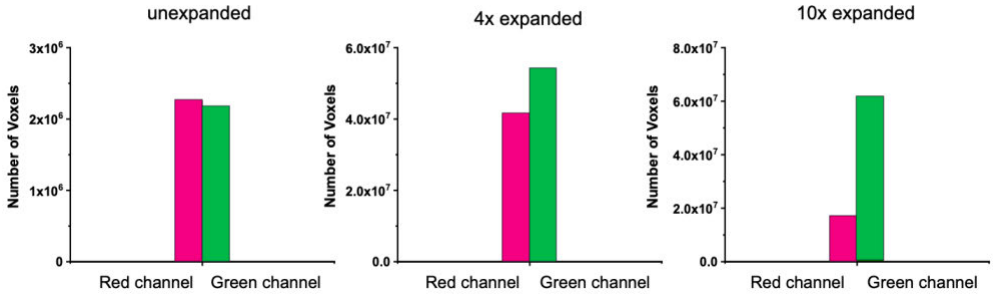

Figure 25: Differences of *N* in two channels. *N* in the red and green channel of unexpanded platelets is quite even (left panel), while in expanded samples *N* strongly differs in the two channels. The labeled receptors correspond to condition I in **Figure 16**. n=30

3.2.2 Expanded platelets with small diameter and diagonal orientation distort colocalization results

Colocalization Analysis is a popular tool for answering biological questions, but for expanded samples no publications exist so far. In expansion microscopy the marked receptors are drifting apart from each other and there is the possibility that graphs imply non – colocalization although it is known that the receptors interact in dependence of one another. To disprove this hypothesis and to validate if colocalization analysis shows reliable results for expansion microscopy, a test experiment has been designed. For this colocalization test case, three conditions are chosen, summarized in Table 13 and **Figure 16**. In the test cases a clear distinction between dependent receptor distribution (high colocalization coefficient), clustered and random, independent receptor organization (low colocalization coefficient) should be visible. For the first condition two different epitopes of the same receptor are labeled, where we expect a very high coefficient close to 1. In the second case, one epitope of a receptor is labeled, but with two different fluorophores. Here, a coefficient between high and low is expected to prove its clustering. The third case is designed to show weak colocalization (coefficient close to 0) so two different receptors are marked which are known to not correlate with one another.[84,85]

As mentioned before, expanded platelets with a diameter less than 12µm are excluded from further analysis to make sure they are not distorting the results due to lower expansion and therefor lower resolution (**Figure 26**). Also, the platelet orientation in the three - dimensional sphere must be considered as the axial resolution of a confocal microscope is ~2.5x worse than the lateral resolution, a diagonal orientated platelet allows a better distinction between markers from the upper and lower platelet membrane reducing the observed colocalization. Therefore, platelets with a diagonal orientation are also excluded from further analysis (**Figure 27**).

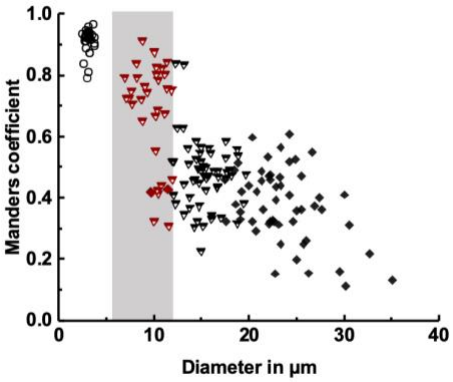

Figure 26: MOC depends on expansion factor. MOC vs. diameter of unexpanded (circles), 4x expanded (triangles) and 10x expanded (diamonds) resting platelets labeled with anti-GPIIb/IIIa ant bodies (5D7) carrying A488 and anti-GPIX antibodies (56F8) carrying A594 (corresponds with condition III in Table 13). Expanded platelets with a diameter below 12µm are excluded from further analysis (marked in red). A modified version of this figure has been pre-published.[84,85]

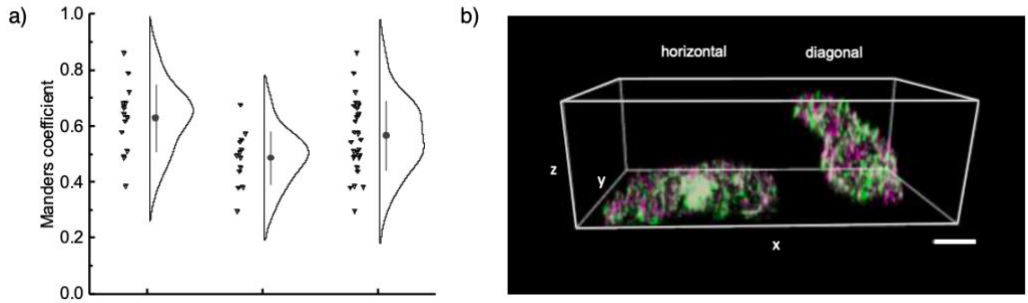

Figure 27: Influence of platelet orientation on MOC. MOC of 4x expanded resting platelets labeled with anti-GPIIb/IIIa antibody (5D7) carrying either Alexa488 (green, right panel) or Alexa594 (magenta, right panel). Diagonal orientated platelets show weaker colocalization than horizontal orientated ones and are excluded from further analysis. Scale bar 4µm. A modified version of this figure has been pre-published.[84,85]

3.2.3 Performance of high and weak colocalization test cases in unexpanded, 4x and 10x expanded resting platelets

After only including platelets with a diameter bigger than 12µm and horizontal orientated, colocalization analysis has been performed. When looking at the colocalization results of unexpanded platelets, in all three cases the coefficient is close to 1 and due to the low resolution, the test cases cannot be distinguished. In expansion the limited signal retention is a real challenge so when looking at expanded platelets it is no surprise that the coefficient in all three cases drops (**Figure 28**).

In 4x expansion, case I shows a value of 0.6 instead of the expected 1, all cases are stretched apart and case I and III can be discriminated now with a dynamic range of 0.15. For 10x platelets this dynamic

range even increases to 0.25 between case I and case III. When looking at the cases, case II is the hardest to interpret. It is lower than the case where we have expected a 100% colocalization but higher than the case where 0% has been predicted.

These results suggest that expansion microscopy differentiates not only colocalization vs. non-colocalization, but also allows discrimination between receptor clustering and random receptor distribution.[84,85]

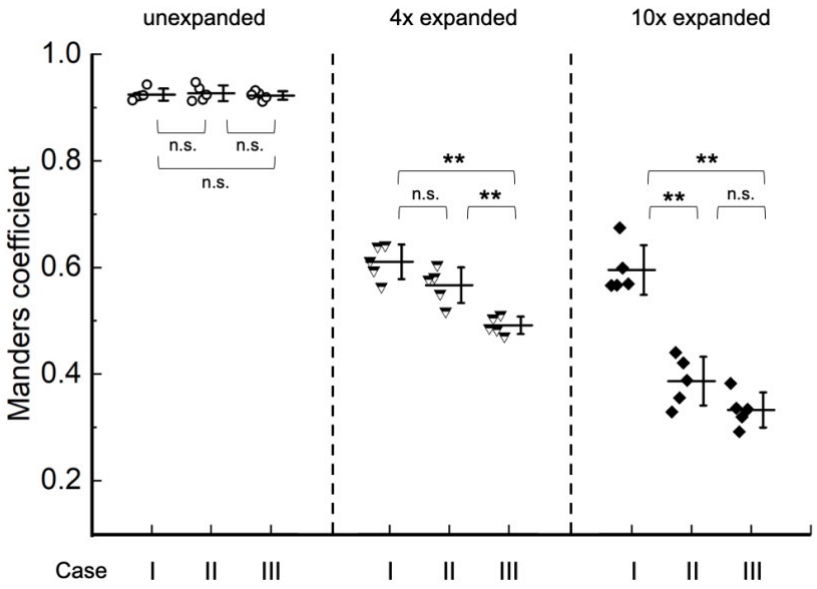

Figure 28: Performance of colocalization test case results based on ExM. Comparing the distributions of the average of MOC of groups of six of unexpanded (left, circles), 4x (middle, triangles) and 10x expanded platelets (right, diamonds) . In unexpanded samples the three cases cannot be distinguished due to lower resolution, while in 4x and 10x samples a clear distinction between condition I and III is shown. n.s.: $p > 0.05$, *: $p \leq 0.05$, **: $p \leq 0.01$, (Kruskal-Wallis ANOVA test), n=30. A modified version of this figure has been pre-published.[84,85]

4 Discussion

Expansion microscopy (ExM) in combination with confocal microscopy has the potential to change the way how platelet receptor-receptor interactions such as clustering, and their distribution can be quantitively measured. The great success of ExM lies in its capability to increase the resolution without the need of any advanced super-resolution setup. The resolution of a standard, confocal microscopy ranges somewhere between 200 – 250*nm* in axial direction and 500*nm* in lateral direction.[45] In combination with ExM biological structures can be resolved within a range of 25 – 100*nm* (axial) and ~60-300*nm* (lateral).[76,77] In comparison, depending on the exact super-resolution approach, resolutions of 40 – 70*nm* have been achieved.[109] Moreover, the combination of ExM and confocal microscopy also outperforms super-resolution microscopes when it comes to 3D and multicolor imaging. Even though this 'super-resolution' approach is not able to detect single molecules – it requires techniques with a resolution power in the nanometer range such as Förster resonance energy transfer (FRET)[110] or electron microscopy[111] – it still allows assumptions about dependent, clustered and independent relationship between receptors on which further investigations can be based on. Densely packed morphologies in tissue and cells such as neurons, microtubules and platelet receptors are challenging to image no matter what optical device is used, simply due to the proximity of structures.

In this thesis, platelets are used as biological targets which again are very small (1—3µm), bear lots of receptors on their surface and get activated easily. In ExM, the homogenously expansion of the polyacrylamide gel by dialysis leads to a drifting apart of receptors from one another, so that the distance between them increases proportionally to the expansion factor allowing sub-diffraction imaging. Therefore, observations of receptor localizations and their distribution on the platelet membrane are more accurate and give insights to still unknown mechanisms making ExM a great tool when it comes to high receptor abundancy.[84,85]

The current, most limiting bottleneck of this technique is that expansion comes at the cost of reduced signal retention and signal dilution. The lower SNR makes it more difficult to discern signal from background, which diminishes the quality of images. In this context, the 10x expansion process has been optimized, modified antibodies have been prepared, imaging modalities/processing have been adjusted and colocalization analysis has been verified by designing test cases of known maximum and minimum colocalization.

The aim has been mapping receptor distributions to draw conclusions regarding the underlying mechanisms of platelet adhesion and aggregation. The potentials and limitations of ExM with blood platelets imaged with a fluorescence confocal microscope will be presented in the following section.

Accuracy and precision of the expansion protocols

The standard expansion protocol[76] ist not designed for blood platelets, so my former colleague, MD student Max Aigner first have had to develop a customized protocol for the platelet context.[84,85] His work mostly deals with protocol improvement and developing the analysis pipeline, while the work of this thesis concentrated on collecting and evaluating more data for a precise, significant colocalization analysis.

Calculation of the expansion factor

Digesting and swelling the sample is quite a harsh manipulation of the sample and can lead to distortions or disruption. Therefore, knowing the expansion factor is playing a pivotal role in the interpretation of the biological meaning of post-expansion images according to their three-dimensional scale. By comparing the size of the same structures or distances between them in pre- and post-expansion images, the F_{ex} and potential distortions can be measured by simply dividing the size of the given post-expansion structure by the size of the identical pre-expansion structure. While post-expansion images are often taken on standard diffraction-limited microscopes, the corresponding landmark positions are set in pre-expansion SRM images.[81,112,110,114] In our experiment it was not possible to compare the exact same platelet but rather the average platelet size before and after expansion, which is referred to as 'microscopic' F_{ex}. Furthermore, the gel diameter is used as reference to calculate the so-called `macroscopic` F_{ex}. When looking at the results, it is noticed that both factors vary a lot, especially in tenfold expansion even though there have been no changes in the protocol. Likewise, the expansion factors between macro- and microscopic diverge extremely. This obvious mismatch is well known, as other papers describe similar findings.[91] One reason that could explain the gap is a bias as for unexpanded platelets bigger platelets (≥3mm) have been chosen over small ones which diminishes the microscopic F_{ex}. Incomplete tissue homogenization could be the reason for both the variation of F_{ex} compared in different experiments and the mismatch between `macroscopic` and `microscopic` F_{ex}. Unintended changes of parameters in the gelation and homogenizing phase such as temperature, pH, duration and enzyme activity could influence gel properties.[91] For a more complete homogenization, Yu et al. proposes to use self-synthesized DNA-oligo-conjugated antibody as used in the original protocol[76] instead of fluorophore-conjugated antibody protocol.[91] When it comes to isotropy or the degree of distortion, it is assumed that the expansion process yields only low, neglectable levels of distortion or rupture, so resolution improves equally in all three dimensions. The isotropic expansion in all directions is required for a credible representation of the sample and has been confirmed by Zhao et al.[112], Chen et al.[76], Tillberg et al.[79] and Yu et al.[91]. Recently, doubts are expressed by Truckenbrodt et al.[77] and Zwettler et al.[90] about preserving the complete 3D molecular architecture. Suggestions that slower speed of tissue homogenization is allowing improved isotropy by giving the polymer network more time to uniformly extend are made by Yu et al.[91] and Gambarotto et al.[115]

Optimization of 10x gel recipe

10x ExM is the cheapest method up to now that can achieve resolutions of 25 – 30*nm* for conventional immunostaining without the use of SRM but epifluorescence microscopy, often just limited by the size of IgG secondary antibodies (~10-15*nm*).[77] This high resolution though comes at the cost of lower signal

retention, a more complex sample preparation than required for fourfold expansion and a diminished mechanical stability of the polymer gel. Truckenbrodt et al.[77] assert that the protocol is highly reproducible and trivially simple whereas I cannot confirm that statement: the gel polymerizing reactions happen rapidly initially – so fast applying and low temperature are necessary – but slow down as soon as gelation has started requiring lots of time for complete polymerization (24h). Additionally, the gel solution must be bubbled with N_2 to exclude oxygen that is inhibiting polymerization. On ground of these challenges, a different, to date unpublished 10x protocol by Tillberg et al. has been given a try to address the mentioned issues. The comparison shows that Truckenbrodt´s gel is thicker and more robust than Tillberg´s which can be explained by the longer gelation duration where Tillberg´s has an advantage because it requires much less time. Truckenbrodt´s macroscopic F_{exp} is higher but surprisingly the platelets inside the gel (=microscopic F_{exp}) are not as much expanded which raises the question if Tillberg´s gel composition is more accessible for proteinase K, the enzyme responsible for digestion (Note: same parameters have been used for both protocols). A major drawback of the comparison is a low number of samples and the missing observation of signal intensities to observe the differences in signal loss/retention. The comparison of signal intensities in 4x and 10x expanded platelets shows unexpected results as the signal retention differs from not only the two dyes but also from the expansion protocol. In general, the signal for the A594 is always lower than the one stained with A488. Against intuition some combinations of antibody/dye show a higher signal intensity in 10x than in 4x expanded platelets. Apparently, there is some sort of chemical reaction or steric conformation that ensures a more efficient linking or prevents antibodies being digested. For increasing the efficiency of protein retention and diminish distortions it is proposed to first execute gel polymerization immediately after Acryloyl-X treatment (=anchoring) and second, to use 150mM $NaHCO_3$ at pH 8.3 instead of PBS as buffer for the anchoring step.[81] According to the denaturation process, Yu et al.[91] suggests to use a buffer containing 40mM $CaCl_2$ that should prevent expansion before the sample is thoroughly digested and therefor minimize distortions. Truckenbrodt et al.[82] use an adjusted digestion buffer containing calcium ions that promote the efficiency of proteinase K activity but might provoke signal loss when anchoring was poor. Ideas to prevent that signal loss are made by Yu et al.[91] and consist in replacing the strong, nonspecific proteinase K with a lighter epitope-preserving permeabilization treatment which consists of adding collagenase and heat mediated digestion in order to reach a gentler homogenization. The careful denaturation comes at the expense of a slightly lower expansion factor and expansion isotropy but has the advantage of preserving more fluorescent signal.[84,85] Washing the gels in a salt-environment (saline sodium citrate buffer, SSC) additionally benefits the stability of staining signals according to Yu et al.[91] In summary, the crux of the expansion protocol is to find the right balance between a high expansion factor, low level of distortion and high signal prevention to produce truthful, valuable data which has the potential to decode unknown structures and mechanisms.

Labeling strategies

There is no doubt that insufficient labeling of studied samples cannot be used as ground for reliable interpretation. Expansion not only comes at the expense of diminished mechanical stability of the gel but also at the cost of an increase in signal dilution. The uneven, `spotty` distribution of fluorescent markers caused by signal dilution and signal loss makes the samples dimmer and reduces the – by

physical expansion achieved – resolution gain. Shi et al.[87] notice a ~83% label loss by proExM, where about 15% are lost in polymerization and about 68% in digestion. To counteract, Max Aigner already has increased the signal retention by replacing PFA with Glyoxal for platelet fixation and using Acryloyl-X instead of Glutaraldehyde as linking solution (unpublished).

To preserve as many labeled fluorophores as possible they need to be strongly attached to the polymer network to survive aggressive denaturation. Modified antibodies are addressing this issue and will be discussed in the further section.

Using modified antibodies to reach higher signal retention

ExM is mainly limited by volumetric signal dilution which is why the aim should be to link as many fluorophores as possible into the gel hopefully surviving homogenization and expansion. This demands establishing tailored protocols that amplify the signal. One of these signal-amplification techniques is the use of antibodies stained with dyes that already contain chemical, non-digestible linkers (see chapter 3.1.4) which has been independently introduced by Wen et al.[89] and Shi et al.[87] This method allows higher fluorophore preservation as the antibody/dye/linker-compound is covalently anchored to the polymer network. The preparation of those modified antibodies for the GPIIb/IIIa and GPIX receptor is quite challenging and only a DOL of maximum 1.9 has been reached which could be explained by steric forces (in comparison, the `normal` dyes A488 and A594 reach DOL´s of up to 4.8). Even though the degree of labeling is lower, the samples stained with modified trifunctional antibodies indeed show higher signal intensity and adding additional linking solution increases signal retention on top. This can be explained by the fact that these produced, modified dyes are relatively new and still need further investigation. It also must be pointed out that the results derive only from one experiment and therefore are not significant for any conclusion, partly because no colocalization analysis has been performed. To date, it cannot be said with certainty if all amenable epitopes are accessible for staining or if the samples are rather saturated. Another drawback is that the market for these special dyes is small and the number of commercially produced trifunctional dyes is currently limited to three: Atto488, Atto561 and Atto647N. Another way to improve not only labeling efficiency but also reduce the linkage error is to stain the sample after digestion/expansion which is called post-expansion labeling.[79,78] Zwettler et al.[90] claim that post-labeling increases the epitope accessibility and diminishes the linkage error proportionally to the expansion factor (from 17.5*nm* to 5*nm*) while others have doubts that all of the epitopes are preserved after homogenization.[82,112] Regarding the linkage error, F_{ab}-fragments outperform the much bigger IgG-antibodies (50kDa vs. 150kDa, respectively)[116] by increasing the localization accuracy and therefor resolution gain of ExM. The downside of F_{ab} - fragments are the reduced labeling density which makes the sample dimmer and only brings benefit in combination with trifunctional dyes. Other strategies for signal improvement are inserting an additional labeling step after gelation using a secondary antibody (`multi-epitope staining`)[117] or by streptavidin staining that is performed iteratively amplified with Hybridization chain reaction (isHCR).[118,119]

Imaging

Imaging of expanded platelets requires not only higher laser power due to dim samples but also longer acquisition time, especially when imaging 10x platelets even though a fast resonant scanner (8000Hz)

is used. Because of the high laser power and long acquisition time, the risk of photobleaching increases which raises the question if there might be microscopes more sensitive to fluorescent signal and therefore more appropriate. The Re-scan microscope (RCM) theoretically has a higher SNR, faster imaging speed and lateral solution is √2 times higher than in confocal microscopy.[120] While my former colleague Max Aigner has tested imaging expanded platelets with RCM finding out that the images in fact showed a much lower SNR likely because of the high noise level of the camera, Gambarotto et. al[121] have succeeded combining ExM and RCM. Fast diffraction limited methods such as light-sheet microscopy are already implemented in the expansion world[122,117] but have the backside of immense datasets that have to be stored and processed.[123] Likewise, the combination of ExM with Super-resolution microscopy remains challenging as specific, complex chemical fixation is required, slow speed is retarding the imaging process and the number of available laser lines limits multicolor imaging.[90,112,124]

Analyzing platelet receptor distributions with Colocalization Analysis

As mentioned, the technique is not a single-molecule approach, so it is doubtful, if the achieved resolution allows imaging single receptors. This makes the interpretation of colocalization results quite difficult since there is always the uncertainty of overlapping signal that can lead to misinterpretation. In a short summary, colocalization is the presentation of overlays of red and green images indicating the relationship between biological molecules or rather giving information about the allocation of molecules/receptors in a certain structure. For colocalization the two most often used coefficients are PCC and MOC. While PCC requires linearity of pixel intensities, MOC is nearly independent of signal proportionality. In the expansion process the signal retention of some antibodies is higher than others so linearity in 4x and 10x is not given and MOC has been chosen. If the labeling with modified antibodies (`trifunctional´) is more homogenous, the more robust PCC is applicable again. Barlow et al.[102] propose to also use thresholded PCC in order to avoid overestimated positive correlation and to allow the demonstration of negative correlation. To avoid the false interpretation of the colocalization results one must have in mind that colocalization does also depend on the receptor density (see section below).

Interpretation of high and low colocalization of GPIIb/IIIa receptors

Regarding the approach, colocalization analysis carries intrinsic challenges: Not only is it not sensitive enough to be claimed as a single molecule technique, it also highly depends on receptor density which in expansion microscopy is diminished due to loss of fluorescent markers. ExM still outweighs the drawbacks since it is an elegant technique to tackle small platelet size and receptor abundancy. For the interpretation, one should bear in mind that a coefficient of 0 (= non-colocalization) also can occur if the labeling density is low whereas a high coefficient might indicate that the expansion factor is not high enough to distinguish densely packed receptors. Therefore, before starting with the calculation, it is necessary to crop out not fully expanded platelets: their high colocalization is a result of the lower resolution. Furthermore, the diagonal orientation of the platelet in the scanning approach leads to less colocalization because of the longer distance between fluorophores.[84,85]

Having potential distortions removed, the analysis results imply pre-formed clustering of GPIIb/IIIa on resting blood platelets which could be responsible for an accelerated response upon vascular injury

caused by an enhanced inside-out activation of GPIIb/IIIa. Moreover, these clusters might suggest already arranged outside-in signalosomes that are paving the way for a rapid integrin-ligand binding. Further research is required to fully understand these receptor interactions not only among one another but also upon the interplay with GPIb-IX-V, GPIa/IIa and the cytoskeleton.

5 Future prospective

The ExM approach has the potential to revolutionize the way highly dense samples such as platelet receptors are imaged, bypassing the acquisition of super-resolution microscopes and reaching nanoscale resolution with conventional diffraction-limited microscopes that capture the emitted fluorescence light. Thereby, robust multicolor, 3D – imaging with regular off-the-shelf dyes is the main benefit. Although not all of them work in expansion,[125] it is still an advantage over the special dyes required for SRM. The results shown in this thesis look promising. Still, there are some bottlenecks that must be considered so the technique can reach its full potentiality. The biggest issue in the expansion process is signal loss through dilution or due to harsh digestion or insufficient linking. The more the sample expands, the less fluorescent signal remains, so higher resolution always comes at the cost of low SNR. A way to surpass the low signal retention is the use of trivalent linked antibodies, although producing them needs a lot of effort, the results have shown its efficiency. However, the number of adequate, currently developed trifunctional dyes is relatively small and limits multicolor imaging.[89] Regarding the linkage error and as a consequence localization precision, IgG antibodies (~ 10-15*nm*), do not reflect the position of molecules as accurately as F_{ab}-fragments (~ 6*nm*). Staining them with trifunctional linked dyes could enhance localization density and precision enormously. Another promising improvement in signal retention is the application of post-expansion labeling where the samples are stained after homogenization/expansion. A gentler homogenization like heat denaturation might prevent potential epitope destruction and lead to lower distortions in the expansion procedure. By combining ExM with SLML it is theoretically feasible to reach the resolution of electron microscopy but there are still current limitations such as the incompatibility of expanded polyelectrolyte hydrogels with photoswitching buffers.[114] When the issue of signal retention is negligibly small, antibodies could be extended to other platelet receptors such as GPIbα (is binding vWF) in order to analyze their relationship to the cytoskeleton or other integrin-ligand binding. Likewise, it would be interesting to image activated platelets and see how colocalization and thus receptor distribution in the platelet membrane changes. The beforementioned ‘non-classical clotting’ and its potential impact on the receptor organizations might be explained this way.[84,85] ExM is an attractive method that enable further insights upon the platelet field to help developing new antithrombotic drugs that only inhibit pathological thrombus formation but not hemostatic processes. In combination with advanced imaging approaches such as SRM and provided a more efficient and accurate labeling (F_{ab}-fragments with trifunctional linkers), ExM has a bright future and may elucidate yet unknown receptor interactions with nanoscale precision.

Appendix

A. Imaging settings

Table 17: Acquisition parameters

	unexpanded samples	expanded samples
Format (px)	1024x1024	1024x1024
Speed (Hz)	8000	8000
Zoom Factor	6	6
Pixel size	41.2	41.2
Line Average	8	8
Line Accumulation	1	1
Frame Average	1	1
Frame Accumulation	1	3
z-step size (µm)	0.17	0.17

Table 18: Settings of Argon laser (wavelength of 488nm)

	unexpanded samples	expanded samples
Laser intensity (%)	4	50
Detector position	500-550	500-550
Gain	100	100

Table 19: Settings of HeNe Laser (wavelength of 594nm)

	unexpanded samples	expanded samples
Laser intensity (%)	10	70
Detector position	605-650	500-550
Gain	100	100

B. Macro file for applying distortion matrix

```
setBatchMode(true);
path = File.openDialog("Select a File");
outpath=getDirectory("Choose a Directory");
run("Bio-Formats Macro Extensions");
Ext.setId(path);
Ext.getCurrentFile(file);
Ext.getSeriesCount(seriesCount);

for (s=1; s<=seriesCount; s++)
{
run("Bio-Formats Importer", "open=&path autoscale color_mode=Default view=Hyperstack stack_order=XYCZT series_"+s);
Ext.getCurrentFile(file);
Ext.setSeries(s-1);
Ext.getSeriesName(seriesName);
Ext.getSeries(seriesName2);
Ext.getSeriesMetadataValue("Series 1 Name", value);
filename = getInfo("image.filename");
windowname = getTitle();
run("Split Channels");
selectWindow("C2-"+windowname);
Stack.getDimensions(width, height, channels, slices, frames);
run("Stack to Images");
selectWindow("C1-"+windowname);
run("Stack to Images");
for (i=1; i<=slices; i++)
{
call("bunwarpj.bUnwarpJ_.loadElasticTransform", "\\\\HC1008\\Users\\AG
Heinze\\\\DATA\\SP5\\2020\\20200211_SM_10x_plat_Coloc_5D7_14A3_56F8\\Calibration\\Averaged shifted
histogram_A561_A488direct_transf.txt", "c:2/2 z:" + i + "/" + slices  + " - "+ seriesName, "c:1/2 z:" + i + "/" + slices  + " - " + seriesName);
selectWindow("c:1/2 z:" + i + "/" + slices  + " - " + seriesName);
setMinAndMax(0, 255);
run("8-bit");
}
run("Images to Stack", "name=StackC1 title=c:1/2 use");
run("Images to Stack", "name=StackC2 title=c:2/2 use");
run("Merge Channels...", "c1=StackC1 c2=StackC2");
run("Make Composite");
Stack.setDisplayMode("grayscale");
run("Arrange Channels...", "new=12");
outpath2 = outpath + filename + seriesName ;
run("OME-TIFF...", "save=["+outpath+filename+seriesName+".ome.tif] export compression=Uncompressed");
}
```

C. Statistics

Table 20: Shapiro-Wilk Test

Manders´overlap coefficient	I	II	III
unexpanded	p=0.01	p=0.59	p=1.66E-4
4x	p=0.19	p=0.95	p=0.23
10x	p=0.13	p=0.58	p=0.40

Table 21: Kruskal-Wallis Test

Manders´overlap coefficient	I vs. II	I vs. III	II vs.III
unexpanded	p=6.55E-5	p=2.86E-5	p=0.89
4x	p=0.16	p=2.23E-6	p=0.01
10x	p=6.51E-6	p=3.01E-10	p=0.29

Bibliography

1. Thon, J. N. *et al.* Cytoskeletal mechanics of proplatelet maturation and platelet release. *J. Cell Biol.* **191**, 861–874 (2010).
2. Jackson, C. W., Steward, S. A., Chenaille, P. J., Ashmun, R. A. & McDonald, T. P. An analysis of megakaryocytopoiesis in the C3H mouse: An animal modal whose megakaryocytes have 32N as the modal DNA class. *Blood* **76**, 690–696 (1990).
3. Eason, C. T., Pattison, A., Howells, D. D., Mitcheson, I. & Bonner, F. W. Platelet population profiles: Significance of species variation and drug-induced changes. *J. Appl. Toxicol.* **6**, 437–441 (1986).
4. Brecher, G. & Cronkite, E. P. Morphology and enumeration of human blood platelets. *J. Appl. Physiol.* **3**, 365–377 (1950).
5. Martin, J. F., Kristensen, S. D., Mathur, A., Grove, E. L. & Choudry, F. A. The causal role of megakaryocyte-platelet hyperactivity in acute coronary syndromes. *Nature Reviews Cardiology* (2012) doi:10.1038/nrcardio.2012.131.
6. Stegner, D. & Nieswandt, B. Platelet receptor signaling in thrombus formation. *Journal of Molecular Medicine* (2011) doi:10.1007/s00109-010-0691-5.
7. Varga-Szabo, D., Pleines, I. & Nieswandt, B. Cell adhesion mechanisms in platelets. *Arteriosclerosis, Thrombosis, and Vascular Biology* **28**, 403–413 (2008).
8. Nieswandt, I. Pleines, M. B. Platelet adhesion and activation mechanisms in arterial thrombosis and ischaemic stroke. **9**, 92–104 (2011).
9. Massberg, S. *et al.* A critical role of platelet adhesion in the initiation of atherosclerotic lesion formation. *J. Exp. Med.* **196**, 887–896 (2002).
10. Horstman, L. L. *et al. Role of platelets in neuroinflammation: a wide-angle perspective*. (2010) doi:10.1186/1742-2094-7-10.
11. Contursi, A. *et al.* Platelets in cancer development and diagnosis. *Biochemical Society Transactions* (2018) doi:10.1042/BST20180159.
12. Jain, S., Harris, J. & Ware, J. Platelets: Linking hemostasis and cancer. *Arterioscler. Thromb. Vasc. Biol.* **30**, 2362–2367 (2010).
13. Volz, J. *et al.* Inhibition of platelet GPVI induces intratumor hemorrhage and increases efficacy of chemotherapy in mice. *Blood* **133**, 2696–2706 (2019).
14. Berger, P. B. *et al.* Bleeding complications with dual antiplatelet therapy among patients with stable vascular disease or risk factors for vascular disease: Results from the clopidogrel for high atherothrombotic risk and ischemic stabilization, management, and avoidance. *Circulation* (2010) doi:10.1161/CIRCULATIONAHA.109.895342.
15. Khurram, Z. *et al.* Combination therapy with aspirin, clopidogrel and warfarin following coronary stenting is associated with a significant risk of bleeding. *J. Invasive Cardiol.* **18**, 162-164 (2006).
16. Ungerer, M. *et al.* Novel Antiplatelet Drug Revacept (Dimeric Glycoprotein VI-Fc) Specifically and Efficiently Inhibited Collagen-Induced Platelet Aggregation Without Affecting General Hemostasis in Humans. *Circulation* **123**, 1891–1899 (2011).
17. Holthenrich, A. & Gerke, V. Regulation of von-willebrand factor secretion from endothelial cells by the annexin a2-s100a10 complex. *International Journal of Molecular Sciences* **19**, 1752 (2018).
18. Ruggeri, Z. M. The role of von Willebrand factor in thrombus formation. *Thromb. Res.* **120**, 5–9 (2007).
19. Broos, K., Feys, H. B., De Meyer, S. F., Vanhoorelbeke, K. & Deckmyn, H. Platelets at work in primary hemostasis. *Blood Rev.* **25**, 155–167 (2011).
20. Clemetson, K. J. Platelets and primary haemostasis. *Thrombosis Research* (2012) doi:10.1016/j.thromres.2011.11.036.

21. Lippi, G., Favaloro, E. J., Franchini, M. & Guidi, G. C. Milestones and perspectives in coagulation and hemostasis. *Seminars in Thrombosis and Hemostasis* (2009) doi:10.1055/s-0029-1214144.
22. Li, Z., Delaney, M. K., O'Brien, K. A. & Du, X. Signaling during platelet adhesion and activation. *Arterioscler. Thromb. Vasc. Biol.* **30**, 2341–2349 (2010).
23. Coller, B. S. & Shattil, S. J. The GPIIb/IIIa (integrin άIIbB3) odyssey: A technology-driven saga of a receptor with twists, turns, and even a bend. *Blood* (2008) doi:10.1182/blood-2008-06-077891.
24. Andrews, R. K. & Berndt, M. C. Platelet adhesion: A game of catch and release. *Journal of Clinical Investigation* **118**, 3009–3011 (2008).
25. FitzGerald, G. A. Mechanisms of platelet activation: Thromboxane A2 as an amplifying signal for other agonists. *Am. J. Cardiol.* (1991) doi:10.1016/0002-9149(91)90379-Y.
26. Luo, S. Z. *et al.* Glycoprotein Ibα forms disulfide bonds with 2 glycoprotein Ibβ subunits in the resting platelet. *Blood* **109**, 603–609 (2007).
27. McEwan, P. A. *et al.* Quaternary organization of GPIb-IX complex and insights into Bernard-Soulier syndrome revealed by the structures of GPIβ and a GPIβ/GPIX chimera. *Blood* **118**, 5292–5301 (2011).
28. Modderman, P. W., Admiraal, L. G., Sonnenberg, A. & Von dem Borne, A. E. G. K. Glycoproteins V and Ib-IX form a noncovalent complex in the platelet membrane. *J. Biol. Chem.* **267**, 364–369 (1992).
29. Estevez, B. & Du, X. New Concepts and Mechanisms of Platelet Activation Signaling. *Physiology* **32**, 162–177 (2017).
30. Bergmeier, W., Rackebrandt, K., Schröder, W., Zirngibl, H. & Nieswandt, B. Structural and functional characterization of the mouse von Willebrand factor receptor GPIb-IX with novel monoclonal antibodies. *Blood* **95**, 886–893 (2000).
31. Nieswandt, B., Bergmeier, W., Rackebrandt, K., Engelbert Gessner, J. & Zirngibl, H. Identification of critical antigen-specific mechanisms in the development of immune thrombocytopenic purpura in mice. *Blood* **96**, 2520–2527 (2000).
32. Nakamura, F. *et al.* The structure of the GPIb-filamin A complex. (2006) doi:10.1182/blood-2005-10.
33. Zeiler, M., Moser, M. & Mann, M. Copy number analysis of the murine platelet proteome spanning the complete abundance range. *Mol. Cell. Proteomics* **13**, 3435–3445 (2014).
34. Dunster, J. L. *et al.* Interspecies differences in protein expression do not impact the spatiotemporal regulation of glycoprotein VI mediated activation. *J. Thromb. Haemost.* (2020) doi:10.1111/jth.14673.
35. Tsien, R. Y. The green fluorescent protein. *Annual Review of Biochemistry* (1998) doi:10.1146/annurev.biochem.67.1.509.
36. Zimmer, M. GFP: From jellyfish to the Nobel prize and beyond. *Chem. Soc. Rev.* **38**, 2823–2832 (2009).
37. Lichtman & Conchello. Fluorescence microscopy: reduced photobleaching of rhodamine and fluorescein protein conjugates by n-propyl gallate. *Science* **217**, 1252 (2005).
38. Croft, W. J. *Under the microscope. A brief history of microscopy*. (World Scientific, 2006).
39. Tonomura, A. Direct observation of thitherto unobservable quantum phenomena by using electrons. *Proc. Natl. Acad. Sci. U. S. A.* (2005) doi:10.1073/pnas.0504720102.
40. Klassen, S. The Photoelectric Effect: Reconstructing the Story for the Physics Classroom. *Science and Education* (2011) doi:10.1007/s11191-009-921 .
41. Mori, Y. Optical properties. in *Powder Technology: Fundamentals of Particles, Powder Beds, and Particle Generation* (2006). doi:10.4324/9781315267548-6.
42. Sanderson, J. Introduction to Light Microscopy. *J. Microsc.* (1999) doi:10.1046/j.1365-2818.1999.0429b.x.
43. Thorn, K. A quick guide to light microscopy in cell biology. *Mol. Biol. Cell* (2016) doi:10.1091/mbc.E15-02-0088.

44. Abbe, E. Beiträge zur Theorie des Mikroskops und der mikroskopischen Wahrnehmung. *Arch. für Mikroskopische Anat.* (1873) doi:10.1007/bf02956173.
45. González, S. & Halpern, A. Laser-scanning confocal microscopy. in *Color Atlas of Melanocytic Lesions of the Skin* (2007). doi:10.1007/978-3-540-35106-1_5.
46. Koops, H. W. P. Correction of axial chromatic aberration improves the contrast transfer in bright-field phase contrast imaging. *Nucl. Inst. Methods Phys. Res. A* (1990) doi:10.1016/0168-9002(90)90634-I.
47. Booth, M. J., Neil, M. A. A., Juškaitis, R. & Wilson, T. Adaptive aberration correction in a confocal microscope. *Proc. Natl. Acad. Sci. U. S. A.* (2002) doi:10.1073/pnas.082544799.
48. Peterson, D. A. Confocal Microscopy. in *Encyclopedia of Movement Disorders* (2010). doi:10.1016/B978-0-12-374105-9.00230-6.
49. Piston, D. W. Concepts in Imaging and Microscopy. Choosing objective lenses: The importance of numerical aperture and magnification in digital optical microscopy. *Biol. Bull.* (1998) doi:10.2307/1542768.
50. Smith, C. L. Basic confocal microscopy. *Curr. Protoc. Neurosci.* (2011) doi:10.1002/0471142301.ns0202s56.
51. Larson, J. M., Schwartz, S. a & Davidson, M. W. Resonant Scanning in Laser Confocal Microscopy. *Nickon Microsc.* (2000).
52. Jonkman, J. & Brown, C. M. Any way you slice it—A comparison of confocal microscopy techniques. *J. Biomol. Tech.* (2015) doi:10.7171/jbt.15-2602-003.
53. Schrader, M., Bahlmann, K., Giese, G. & Hell, S. W. 4Pi-confocal imaging in fixed biological specimens. *Biophys. J.* **75**, 1659–1668 (1998).
54. Schermelleh, L. *et al.* Super-resolution microscopy demystified. *Nat. Cell Biol.* **21**, 72–84 (2019).
55. Rust, M. J., Bates, M. & Zhuang, X. Sub-diffraction-limit imaging by stochastic optical reconstruction microscopy (STORM). *Nat. Methods* (2006) doi:10.1038/nmeth929.
56. Betzig, E. *et al.* Imaging intracellular fluorescent proteins at nanometer resolution. *Science* (2006) doi:10.1126/science.1127344.
57. Hess, S. T., Girirajan, T. P. K. & Mason, M. D. Ultra-high resolution imaging by fluorescence photoactivation localization microscopy. *Biophys. J.* (2006) doi:10.1529/biophysj.106.091116.
58. Wegel, E. *et al.* Imaging cellular structures in super-resolution with SIM, STED and Localisation Microscopy: A practical comparison. *Sci. Rep.* **6**, 1–13 (2016).
59. Hirvonen, L. M., Wicker, K., Mandula, O. & Heintzmann, R. Structured illumination microscopy of a living cell. *Eur. Biophys. J.* (2009) doi:10.1007/s00249-009-0501-6.
60. Schermelleh, L. *et al.* Subdiffraction multicolor imaging of the nuclear periphery with 3D structured illumination microscopy. *Science* (2008) doi:10.1126/science.1156947.
61. Wu, Y. & Shroff, H. Faster, sharper, and deeper: structured illumination microscopy for biological imaging. *Nature Methods* (2018) doi:10.1038/s41592-018-0211-z.
62. Hell, S. W. & Wichmann, J. Breaking the diffraction resolution limit by stimulated emission: stimulated-emission-depletion fluorescence microscopy. *Opt. Lett.* (1994) doi:10.1364/ol.19.000780.
63. Klar, T. A., Jakobs, S., Dyba, M., Egner, A. & Hell, S. W. Fluorescence microscopy with diffraction resolution barrier broken by stimulated emission. *Proc. Natl. Acad. Sci. U. S. A.* (2000) doi:10.1073/pnas.97.15.8206.
64. Dyba, M., Jakobs, S. & Hell, S. W. Immunofluorescence stimulated emission depletion microscopy. *Nat. Biotechnol.* (2003) doi:10.1038/nbt897.
65. Hell, S. W. *et al.* The 2015 super-resolution microscopy roadmap. *Journal of Physics D: Applied Physics* (2015) doi:10.1088/0022-3727/48/44/443001.

66. Sidenstein, S. C. *et al.* Multicolour multilevel STED nanoscopy of actin/spectrin organization at synapses. *Sci. Rep.* (2016) doi:10.1038/srep26725.
67. Willig, K. I. *et al.* Nanoscale resolution in GFP-based microscopy. *Nat. Methods* (2006) doi:10.1038/nmeth922.
68. Westphal, V. *et al.* Video-rate far-field optical nanoscopy dissects synaptic vesicle movement. *Science* (2008) doi:10.1126/science.1154228.
69. Donnert, G. *et al.* Macromolecular-scale resolution in biological fluorescence microscopy. *Proc. Natl. Acad. Sci. U. S. A.* (2006) doi:10.1073/pnas.0604965103.
70. Tønnesen, J., Inavalli, V. V. G. K. & Nägerl, U. V. Super-Resolution Imaging of the Extracellular Space in Living Brain Tissue. *Cell* (2018) doi:10.1016/j.cell.2018.02.007.
71. Lidke, K. A. & Heintzmann, R. Localization fluorescence microscopy using quantum dot blinking. in *2007 4th IEEE International Symposium on Biomedical Imaging: From Nano to Macro - Proceedings* (2007). doi:10.1109/ISBI.2007.357007.
72. Henriques, R., Griffiths, C., Rego, E. H. & Mhlanga, M. M. PALM and STORM: Unlocking live-cell super-resolution. *Biopolymers* (2011) doi:10.1002/bip.21586.
73. Ehmann, N., Sauer, M. & Kittel, R. J. Super-resolution microscopy of the synaptic active zone. *Front. Cell. Neurosci.* (2015) doi:10.3389/fncel.2015.00007.
74. Schnitzbauer, J., Strauss, M. T., Schlichthaerle, T., Schueder, F. & Jungmann, R. Super-resolution microscopy with DNA-PAINT. *Nat. Protoc.* (2017) doi:10.1038/nprot.2017.024.
75. Grove, J. Super-resolution microscopy: A virus' eye view of the cell. *Viruses* (2014) doi:10.3390/v6031365.
76. Chen, F., Tillberg, P. W. & Boyden, E. S. Expansion microscopy. *Science* **347**, 543–548 (2015).
77. Truckenbrodt, S. *et al.* X10 expansion microscopy enables 25-nm resolution on conventional microscopes. *EMBO Rep.* **19**, 1–12 (2018).
78. Gambarotto, D. *et al.* Imaging cellular ultrastructures using expansion microscopy (U-ExM). *Nat. Methods* **16**, 71–74 (2019).
79. Tillberg, P. W. *et al.* Protein-retention expansion microscopy of cells and tissues labeled using standard fluorescent proteins and antibodies. *Nat. Biotechnol.* **34**, 987–992 (2016).
80. Chang, J. B. *et al.* Iterative expansion microscopy. *Nat. Methods* **14**, (2017).
81. Truckenbrodt, S. *et al.* X10 expansion microscopy enables 25-nm resolution on conventional microscopes. *EMBO Rep.* **19**, 1–22 (2018).
82. Truckenbrodt, S., Sommer, C., Rizzoli, S. O. & Danzl, J. G. A practical guide to optimization in X10 expansion microscopy. *Nat. Protoc.* **14**, 832–863 (2019).
83. Ahmad, S. Expansion Microscopy on Blood Platelets. (2018).
84. Heil, H. S. *et al.* Mapping densely packed αIIbβ3 receptors in murine blood platelets with expansion microscopy. *bioRxiv* (2021) doi:10.1101/2021.02.16.431449.
85. Heil, H. S. *et al.* Mapping densely packed αIIbβ3 receptors in murine blood platelets with expansion microscopy. *Platelets* (2022) doi:10.1080/09537104.2021.2023735.
86. Richter, K. N. *et al.* Glyoxal as an alternative fixative to formaldehyde in immunostaining and super-resolution microscopy. *EMBO J.* **37**, 139–159 (2018).
87. Shi, X. *et al.* Label-retention expansion microscopy. doi:10.1101/687954.
88. Krishnaswami, V. *et al.* Spatially-controlled illumination with rescan confocal microscopy enhances image quality, resolution and reduces photodamage. in *Three-Dimensional and Multidimensional Microscopy: Image Acquisition and Processing XXIV* (2017). doi:10.1117/12.2251329.
89. Wen, G. *et al.* Evaluation of direct grafting strategies in Expansion Microscopy. (2019) doi:10.1101/696039.
90. Zwettler, F. U. *et al.* Tracking down the molecular architecture of the syn onemal complex by expansion microscopy. *Nat. Commun.* (2020) doi:10.1038/s41467-020-17017-7.
91. Yu, C. C. *et al.* Expansion microscopy of c. Elegans. *Elife* **9**, 1–78 (2020).
92. Li, R., Chen, X., Lin, Z., Wang, Y. & Sun, Y. Expansion enhanced nanoscopy.

Nanoscale **10**, 17552–17556 (2018).
93. Zwettler, F. U., Reinhard, S. & Sauer, M. Ex-dSTORM and automated quantitative image analysis of expanded filamentous structures. in *Methods in Cell Biology* (2020). doi:10.1016/bs.mcb.2020.05.004.
94. Halpern, A. R., Alas, G. C. M., Chozinski, T. J., Paredez, A. R. & Vaughan, J. C. Hybrid Structured Illumination Expansion Microscopy Reveals Microbial Cytoskeleton Organization. *ACS Nano* **11**, 12677–12686 (2017).
95. Cahoon, C. K. *et al.* Superresolution expansion microscopy reveals the three-dimensional organization of the Drosophila synaptonemal complex. *Proc. Natl. Acad. Sci. U. S. A.* **114**, E6857–E6866 (2017).
96. Aaron, J. S., Taylor, A. B. & Chew, T. L. Image co-localization - co-occurrence versus correlation. *Journal of cell science* vol. 131 (2018).
97. Bolte, S. & Cordelières, F. P. A guided tour into subcellular colocalization analysis in light microscopy. *J. Microsc.* **224**, 213–232 (2006).
98. Jonkman, J., Brown, C. M., Wright, G. D., Anderson, K. I. & North, A. J. Tutorial: guidance for quantitative confocal microscopy. *Nat. Protoc.* **15**, 1585–1611 (2020).
99. Sibarita, J. B. Deconvolution microscopy. *Advances in Biochemical Engineering/Biotechnology* (2005) doi:10.1007/b102215.
100. Pearson, K. VII. Mathematical contributions to the theory of evolution.—III. Regression, heredity, and panmixia. *Philos. Trans. R. Soc. London. Ser. A, Contain. Pap. a Math. or Phys. Character* **187**, 253–318 (1896).
101. E.M.M.Manders, J.Stap, G.J.Brakenhoff, R.van Driel, J. A. A. Dynamics of three-dimensional replication patterns during the S-phase, analysed by double labelling of DNA and confocal microscopy. *J. Cell Sci.* **103**, 857–862 (1992).
102. Barlow, A. L., MacLeod, A., Noppen, S., Sanderson, J. & Guérin, C. J. Colocalization analysis in fluorescence micrographs: Verification of a more accurate calculation of Pearson's correlation coefficient. in *Microscopy and Microanalysis* **16**, 710–724 (Cambridge University Press, 2010).
103. Dunn, K. W., Kamocka, M. M. & McDonald, J. H. A practical guide to evaluating colocalization in biological microscopy. *American Journal of Physiology - Cell Physiology* vol. 300 723–742 (2011).
104. Massberg, S. *et al.* A critical role of platelet adhesion in the initiation of atherosclerotic lesion formation. *J. Exp. Med.* (2002) doi:10.1084/jem.20012044.
105. Iizuka, K., Ikebe, M., Somlyo, A. V. & Somlyo, A. P. Introduction of high molecular weight (IgG) proteins into receptor coupled, permeabilized smooth muscle. *Cell Calcium* **16**, 431–445 (1994).
106. Rueden, C. T. *et al.* ImageJ2: ImageJ for the next generation of scientific image data. *BMC Bioinformatics* **18**, 1–26 (2017).
107. Ovesny, M., Kříž ek, P., Borkovec, J., ˇ vindrych, Z. S. & Hagen, G. M. Bioimage informatics ThunderSTORM: a comprehensive ImageJ plug-in for PALM and STORM data analysis and super-resolution imaging. **30**, 2389–2390 (2014).
108. Oscar Sorzano, C. S., Kybic, J., Arganda-Carreras, I., S Sorzano, C. O. & Ortiz-de-Solorzano, C. *bUnwarpJ: Consistent and Elastic Registration in ImageJ. Methods and Applications* **12** (2018).
109. Schermelleh, L., Heintzmann, R. & Leonhardt, H. A guide to super-resolution fluorescence microscopy. *Journal of Cell Biology* **190**, 165–175 (2010).
110. Wu, L. *et al.* Förster resonance energy transfer (FRET)-based small-mol ıle sensors and imaging agents. *Chem. Soc. Rev.* **49**, 5110–5139 (2020).
111. De Jonge, N., Peckys, D. B., Kremers, G. J. & Piston, D. W. Electron mic ɜcopy of whole cells in liquid with nanometer resolution. *Proc. Natl. Acad. Sci. U. S. A.* **106**, 2159–2164 (2009).
112. Zhao, Y. *et al.* Nanoscale imaging of clinical specimens using pathology-optimized expansion microscopy. *Nat. Biotechnol.* **35**, (2017).
113. Scheible, M. B. & Tinnefeld, P. Quantifying Expansion Microscopy with DNA Origami Expansion Nanorulers. *bioRxiv* 265405 (2018) doi:10.1101/265405.

114. Zwettler, F. U. *et al.* Molecular resolution imaging by post-labeling expansion single-molecule localization microscopy (Ex-SMLM). *Nat. Commun.* **11**, 1–11 (2020).
115. Gambarotto, D., Zwettler, F. U., Cernohorska, M., Fortun, D. & Borgers, S. Imaging beyond the super - resolution limits using ultrastructure expansion microscopy (UltraExM). *BioRxiv* (2018) doi:10.1101/308270.
116. Wu, A. M. & Senter, P. D. Arming antibodies: prospects and challenges for immunoconjugates. *Nat. Biotechnol.* **23**, 1137–1146 (2005).
117. Gao, R. *et al.* Cortical column and whole-brain imaging with molecular contrast and nanoscale resolution. *Science* **363**, (2019).
118. Lin, R. *et al.* A hybridization-chain-reaction-based method for amplifying immunosignals. *Nat. Methods* **15**, 275–278 (2018).
119. Sun, D. en *et al.* Click-ExM enables expansion microscopy for all biomolecules. *Nat. Methods* **18**, 107–113 (2021).
120. de Luca, G. M. R. *et al.* Configurations of the Re-scan Confocal Microscope (RCM) for biomedical applications. *J. Microsc.* **266**, 166–177 (2017).
121. Gambarotto, D. *et al.* Imaging cellular ultrastructures using expansion microscopy (U-ExM). *Nat. Methods* **16**, 71–74 (2019).
122. Chen, F. *et al.* Nanoscale imaging of RNA with expansion microscopy. *Nat. Methods* (2016) doi:10.1038/nmeth.3899.
123. Watkins, S. C. & St. Croix, C. M. Light sheet imaging comes of age. *J. Cell Biol.* **217**, 1567–1569 (2018).
124. Zwettler, F. U. *et al.* Tracking down the molecular architecture of the synaptonemal complex by expansion microscopy. *bioRxiv* (2019) doi:10.1101/821298.
125. Chozinski, T. J. *et al.* Expansion microscopy with conventional antibodies and fluorescent proteins. *Nat. Methods* **13**, 485–488 (2016).

Acknowledgement

First, I must thank Katrin for giving me the chance to peek into the world of science. Not only are you an exceptional scientist, colleague, and mentor to anyone who works with you but an admirable person with great strength, courage, and sense of humor.

I would also like to thank Markus Sauer und Harald Schulze, my other two supervisors on the thesis committee, for their support and helpful input during our committee meetings. It once again showed me how the exchange of knowledge enriches everyday life.

Next, I must thank Hannah. For everything. Your dedication and attention to every single detail is truly extraordinary and it is very hard to resist your scientific enthusiasm. Thank you for showing me how to do proper literature research, preparing me for talks and for proofreading, of course. You are the best supervisor I could have wished for.

A big thank you goes to Max, my predecessor on this project, who put so much effort in developing the expansion protocols and setting the parameters for data analysis. Also, thank you, Luise and Prateek, for carrying on with the project so successfully.

I must thank Christoph for showing me how the experiments are performed and Bernhard Nieswandt for letting me use his antibodies. David, Vanessa and Charly and Timo: Thank you for helping me out with all matters regarding platelet biology whether by recommending useful papers, proofreading, or bleeding mice for me.

A huge thank you goes to the Heinze Lab, who gave me a warm welcome and always made me feel supported during my time there. Especially, I would like to thank Jan for explaining me statistical, physical, and mathematical issues in easy words and for giving me helpful advice regarding the structure of this thesis. Katherina, thank you for helping me with the data analysis and for checking my calculations. I must thank Mike and Jürgen for their microscopic expertise when there was just a black screen instead of fluorescent signal. Also, thank you to all other members at that time: Ash, Susobhan, Deyan, Johannes, Kerstin, Christine. You made my lab time much more enjoyable, especially during lunch break.

I also must thank members of the Sauer Lab, in particular Jan Schlegel for letting us use his resonant scanner and sharing his knowledge.

Finally, I would like to thank my family and friends! Without their love and support I would not be the person I am today.

Curriculum vitae

Affidavit

I hereby confirm that my thesis entitled *"Mapping membrane receptor distribution on resting platelets combining Expansion Microscopy and fluorescence confocal microscopy"* is the result of my own work. I did not receive any help or support from commercial consultants. All sources and/or materials applied are listed and specified in the thesis.

Furthermore, I confirm that this thesis has not yet been submitted as part of another examination process neither in identical nor in similar form.

München …..……. Signature …..…….

Eidesstattliche Erklärung

Hiermit erkläre ich an Eides statt, dass die Dissertation *„Kartierung der Membranrezeptorverteilung auf nicht-aktivierten Blutplättchen mithilfe der Kombination aus Expansionsmikroskopie und konfokaler Fluoreszenzmikroskopie“* eigenständig, d.h. insbesondere selbständig und ohne Hilfe eines kommerziellen Promotionsberaters, angefertigt und keine anderen als die von mir angegebenen Quellen und Hilfsmittel verwendet wurden.

Ich erkläre außerdem, dass die Dissertation weder in gleicher noch in ähnlicher Form bereits in einem anderen Prüfungsverfahren vorgelegen wurde.

München …..……. Signature …..…….